Universidade de Aveiro Departamento de Química
Ano lectivo 2009/2010

Maria João Marques de Carvalho

CARACTERIZAÇÃO DE UM DOMÍNIO DO C-TERMINAL DE UM CANAL DE POTÁSSIO

CHARACTERIZATION OF A C-TERMINAL DOMAIN FROM EAG POTASSIUM CHANNEL

Universidade de Aveiro Departamento de Química
Ano lectivo 2009/2010

Maria João Marques de Carvalho

CHARACTERIZATION OF A C-TERMINAL DOMAIN FROM EAG POTASSIUM CHANNEL

Dissertação apresentada à Universidade de Aveiro para cumprimento dos requisitos necessários à obtenção do grau de Mestre em Métodos Biomoleculares, realizada sob a orientação científica do Doutor João Morais-Cabral do Instituto de Biologia Molecular e Celular e sob a co-orientação científica do Doutor Vítor Félix, Professor Associado do Departamento de Química da Universidade de Aveiro

Apoio financeiro a J. Morais-Cabral da Fundação para a Ciência e Tecnologia (FCOMP - 010124-FEDER-007427/PTDC/QUI/66171/2006)

o júri

presidente

Prof. Doutor Pedro Domingues
professor auxiliar da Universidade de Aveiro

Prof. Doutor Brian J.Goodfellow
professor auxiliar da Universidade de Aveiro

Prof. Doutor Vítor Félix
professor associado da Universidade de Aveiro

Doutor João Morais-Cabral
investigador principal no Instituto de Biologia Molecular e Celular

agradecimentos

Gostaria de agradecer ao meu orientador Dr. João Morais-Cabral e à Dra. Carol Harley por todo o apoio que me deram e pelas técnicas que me proporcionaram aprender durante o meu projecto de mestrado . Também queria agradecer ao Prof. Vítor Felix por ter aceite ser meu orientador interno.

Obrigada ao meu amigo e colega Ricardo Adaixo pelas inúmeras discussões e conhecimentos partilhados. Já me fazes falta!
Ricardo Pires, obrigada por estares sempre disponível para aconselhar e ajudar.

Obrigada ainda aos restantes companheiros de laboratório.

Por fim, obrigada Sérgio, amigos e família por aturarem o meu mau humor quando as coisas não corriam bem.

palavras-chave EAG, domínios que ligam nucleotideos cíclicos, cristalografia, calmodulina

resumo

Domínios que ligam nucleotideos cíclicos (CNBD) regulam muitas vias de sinalização em células procarióticas e eucarióticas. Os ligandos AMP cíclico ou GMP cíclico ligam-se a estes domínios e induzem uma alteração conformacional que é propagada ao domínio efector, como uma cinase ou um canal iónico.

Os canais de potássio da família *ether-a-go-go* (EAG) estão envolvidos em muitos processos fisiológicos que incluem repolarização cardíaca e neuronal, proliferação tumoral e secreção de hormonas. Estes canais são tetraméricos e cada subunidade inclui seis hélices transmembranares e dominios citoplasmáticos em N- e C-terminal. O domínio em C-terminal tem homologia com domínios que ligam nucleotídeos cíclicos mas foi demonstrado que os canais EAG não são afectados por nucleotídeos e o domínio não liga nucleotideos. O objectivo deste projecto foi resolver a estrutura de um domínio C-terminal de um canal EAG por cristalografia de raios-X e compreender o seu papel funcional. Determinei a estrutura de um destes domínios à resolução de 2,2 Å; a estrutura tem a topologia de um CNBD mas a cavidade de ligação apresenta várias diferenças relativamente à de domínios que ligam nucleotideos cíclicos. Mais ainda, os canais EAG são inibidos por calmodulina e há dois locais de ligação de calmodulina a seguir ao CNBD. A estrutura mostrou que um destes locais se encontra sobreposto com uma região do domínio levantando a possibilidade da calmodulina regular o canal através da alteração conformacional do domínio C-terminal dos canais EAG. Esta possibilidade começou a ser explorada com recurso a ensaios de *cross-linking* químico e espectroscopia de fluorescência.

keywords EAG, cyclic nucleotide binding domain, crystallography, calmodulin

abstract

Cyclic nucleotide binding domains (CNBD) are regulatory domains that participate in many signaling pathways in prokaryotic and eukaryotic cells. The ligand cAMP or cGMP binds these domains and induces a conformational change that is propagated to an effector domain, like a kinase or an ion channel.

The ether-a-go-go (EAG) potassium channel family is involved in important physiological roles that include cardiac and neuronal repolarization, tumor proliferation and hormone secretion. These channels are tetramers, where each subunit includes six transmembrane helices and N- and C-terminal cytoplasmic domains. The C-terminal domain has strong homology to CNBDs but it has been demonstrated that EAG channels are not affected by cyclic nucleotides and that the domain does not bind nucleotides. The ultimate goal of this project was to solve the structure of an EAG family C-terminal domain by X-ray crystallography and to understand its functional role. I have determined the structure of one of these domains at 2.2 Å; the structure has the canonical CNBD fold but it shows a ligand pocket that has several differences relative to a cyclic nucleotide binding site. Furthermore, EAG currents are inhibited by calmodulin binding and there are two calmodulin binding sites C-terminal to the CNBD. The structure reveals that one of these sites overlaps with a region of the domain raising the possibility that calmodulin affects channel function by changing the EAG C-terminal domain conformation. I have conducted preliminary tests on this hypothesis by using biochemical cross-linking experiments and fluorescence spectroscopy.

Contents

Abbreviations

cAMP and cGMP - cyclic adenosine monophosphate and cyclic guanosine monophosphate

CCP4 - Collaborative Computational Project 4

CNG - cyclic nucleotide-gated channel

CNBD - cyclic nucleotide binding domain

DNA - deoxyribonucleic acid

DTSSP - 3,3´-dithiobis[sulfosuccinimidylpropionate]

DTT - dithiothreitol

EAG - ether à go-go

EDTA- ethylenediaminetetraacetic acid

EGS - ethylglycol bis(succinimidylsuccinate)

ESRF - European Synchrotron Radiation Facility

hCaM - human calmodulin

HCN - hyperpolarization-activated cyclic nucleotide-modulated channel

HEPES- 4-(2-hydroxyethyl)-1-piperazineethanesulfonic acid

IMAC - immobilized metal affinity chromatography

IPTG - isopropyl β-D-1-thiogalactopyranoside

kbp - kilo base pair

LB - Luria-Bertania Broth

MCS - multiple cloning site

mEAG - mouse eag

MlotiK - *Mesorhizobium loti* K^+ channel

OD - optical density

PEG- polyethylene glycol

PCR - polymerase chain reaction

PDB - Protein Data Bank

PMSF- phenylmethanesulphonylfluoride

SDS-PAGE- sodium dodecyl sulfate polyacrylamid gel electrophoresis

Tris- tris(hydroxymethyl)aminomethane

Introduction

Ion transport across biological membranes

Biological membranes are mostly impermeable to polar or charged solutes. Transport of ions through lipid membranes must consequently be mediated by transmembrane proteins that prevent the contact of the ions with the hydrophobic interior of the phospholipidic bilayer. This transport can either occur by diffusion of an ion down its electrochemical gradient (facilitated diffusion) or against its electrochemical potential, with an associated energy cost (active transport) [1,2].

These transport proteins can be classified as pumps, transporters or channels. Pumps are, for example, ATPases that use the energy from ATP hydrolysis to move ions against their electrochemical potential. Transporters are further divided into uniporters that move a single molecule down its gradient, and symporters and antiporters that couple the transport of one molecule uphill to another one downhill. Transport in channels occurs by facilitated diffusion; furthermore, channels can allow ion movement at much higher rates than any of the transport systems [1,2].

Ion channels

Ion channels (calcium, sodium, chloride or potassium channels) are present in all eukaryotic cells' plasma membranes and together with ion pumps are responsible for the maintenance of the resting membrane potential at ~-70mV.

Besides having rates of transport near the unrestricted diffusion (up to 10^8 ions/s), ion channels are not saturable, most of them show selectivity for particular ions and are gated, switching between open and closed states in response to a stimuli that can be membrane voltage or the concentration of a ligand or ion.

Gating domains (voltage sensors or ligand binding domains) transform a stimulus into pore opening. The basic function of a voltage sensor domain is to couple movement of protein charges to pore opening, in response to changes the membrane electric field.

In channels with six transmembrane segments the voltage sensor is located mostly on the fourth transmembrane helix (S4) and is composed of positively charged residues at every third position [3]. In ligand-gated channels, the binding of a ligand (for example, cyclic nucleotide) will induce conformational changes that are transmitted to the pore region and favour the open state.

EAG K^+ channel family

Ether à go-go (EAG) channels are voltage-gated potassium channels involved in many important physiological phenomena such as cardiac and neuronal repolarization, insulin secretion, cell differentiation and tumor growth.

The typical K^+ channel is an assembly of four subunits (tetramer) surrounding a central pore with a four-fold symmetry, fig. 1B. It can have two or six transmembrane helices as well as cytoplasmic regulatory/gating domains [4,5].

Potassium channels contain a highly conserved signature sequence in the pore region (GYG or GFG – selectivity filter) that forms the coordinating shell for potassium ions in the channel. This region is responsible for the high selectivity of K^+ ion over the Na^+ ion by a factor of over 1000 [6]. Mutation of these residues disrupts the channel's ability to discriminate between K^+ and Na^+ ions [4,5]

The eag gene was first identified by a mutation that gave *Drosophila melanogaster* leg shaking behavior when under ether anesthesia, hence the name [7]. Using homology screens of cDNA libraries, three related gene subfamilies have been found – eag, erg (eag-related gene) and elk (eag-like K^+ channel), fig. 1C.

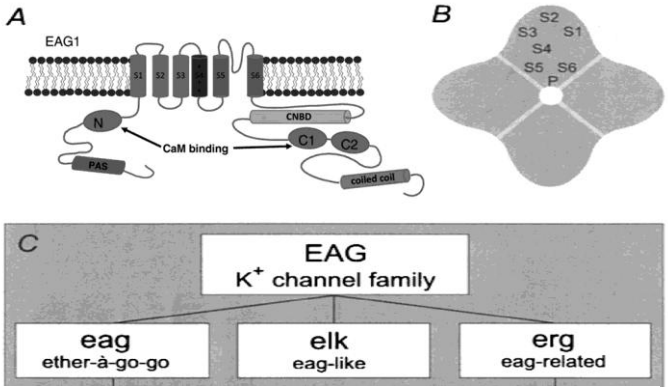

Fig. 1 - The EAG potassium channel family. A – Schematic representation of an α-subunit of an EAG channel, composed of an N-terminal PAS domain, followed by a 6TM arrangement and a C-terminal putative CNBD; B – Proposed arrangement of a tetrameric 6 TM K^+ channel; C – Three subfamilies of EAG K^+ channel family. Adapted from [38] and Heinemann, SH.

Sequence alignments show that members of the EAG family are closely related to cyclic nucleotide-gated cation channels as well as voltage-gated K^+ channels [8]. In particular, the human ERG potassium channel has great clinical importance since a set of inherited channel mutations give rise to long QT syndrome (LQTS), a condition characterized by arrhythmia, seizures and sudden death. However, the most common form of LQTS is acquired and is induced by drugs that block the channel, disrupting its normal function.

EAG channels contain an N-terminal Per-Arnt-Sim (PAS) and a C-terminal putative cyclic nucleotide binding domain (CNBD) in addition to the characteristic six transmembrane helices (S1-S6) fold of voltage-gated K^+ channels, fig. 1A. PAS and CNBD are cytosolic ligand binding domains and are thought to play important roles in these channels. However, their function is not fully understood nor have ligands been reported for either of these regulatory domains [9].

Cyclic nucleotide binding domains (CNBDs)

Cyclic nucleotide binding domains regulate signaling pathways in both eukaryotes and prokaryotes. These domains bind cAMP or cGMP and can be found in the bacterial catabolic activated protein (CAP, the first CNBD structure to be reported), or the eukaryotic nucleotide exchange factor (Epac), protein kinases (PKA, PKG) [10], and cyclic nucleotide-regulated channels (hyperpolarization-activated cyclic nucleotide-modulated channel – HCN [11] and cyclic nucleotide-gated channel - CNG).

Structurally, CNBDs are composed of an antiparallel β-roll of eight β-strands preceded by an α-helix (αA) and followed by α-helices αB ("hinge") and αC ("lid"), fig. 2 and

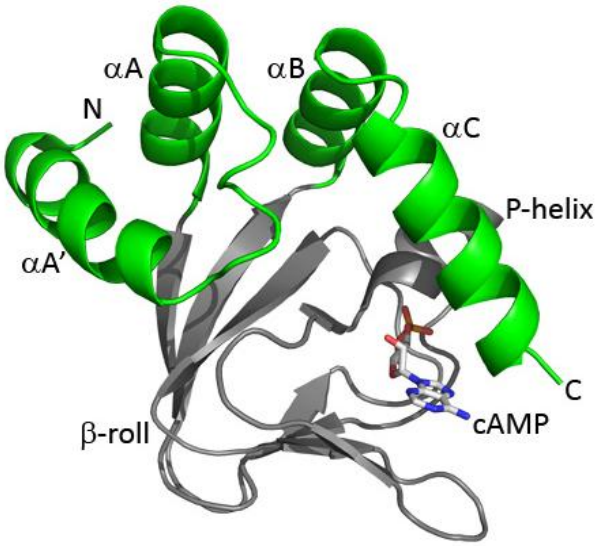

Fig. 2 - Wild-type structure of MlotiK CNBD with cAMP. Ligand is shown in stick model, β-roll and P-helix are in grey. PDB code 1VP6 [16].

Appendix I for multiple sequence alignment of mEAG, hEAG, HERG, mHCN2 and MlotiK. In cyclic nucleotide-regulated channels, extra helices (fig. 2 and Appendix I) connect the channel pore to the CNBD and are responsible for transmitting the cAMP-induced conformation change to the pore; this region is known as the C-linker. An additional short α-helix, P-helix, is located between β-strands 6 and 7 and is part of a key structural region - the phosphate binding cassette, PBC - that anchors the phosphate group of the cyclic nucleotide. There are several key residues involved in ligand coordination including the PBC's glutamate, arginine and serine/threonine, fig. 3. The glutamate forms a hydrogen bond with the ribose, the serine/threonine interacts with the oxygens of the phosphate group of cAMP and the arginine forms a salt bridge with the phosphate, fig. 3 and Appendix I [11,12]. Mutations on the PBC's arginine in MlotiK [13], mHCN2 [14] and CNG decreased cyclic nucleotide binding affinity, but still allowed for cyclic nucleotide modulation in these channels. The lid region interacts with the base of the nucleotide through an arginine, tyrosine or tryptophan, fig. 3. Note that some domains adopt the CNBD fold without a canonical PBC and have gained the ability to bind other ligands, like the group heme in the case of CooA transcription activator [15].

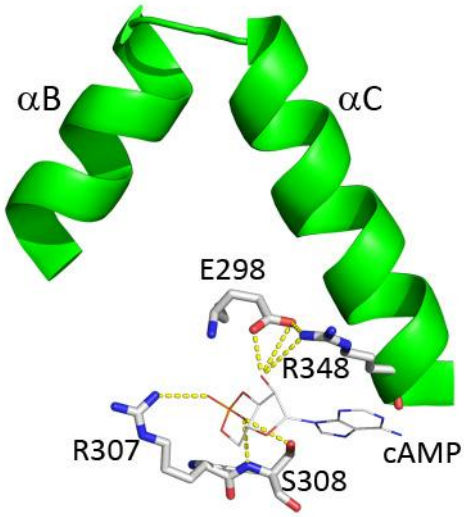

Fig. 3 - Close up of the residues of PBC (Glu298, Arg307, Ser308) and helix C that coordinate cAMP (Arg348) in MlotiK and. PDB code 1VP6 [16].

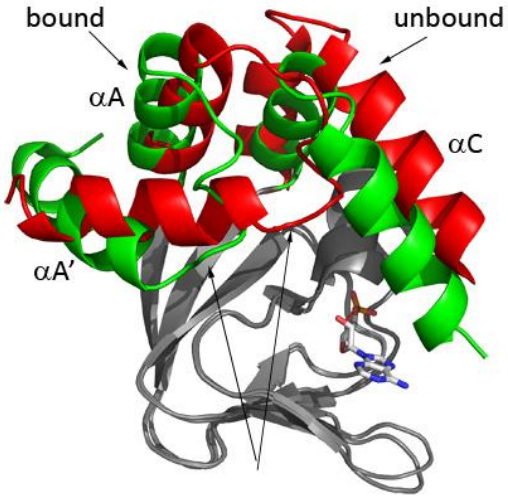

Fig. 4 - Superposition between liganded (PDB code 1VP6, cAMP in stick model, β-roll in grey, α-helices in green) and unliganded structures of MlotiK CNBD (PDB code 1U12, β-roll in grey, α-helices in red). Large arrows indicate two positions of loop between αA'-αA.

The CNBD of the bacterial channel MlotiK provides a good model for understanding the mechanism behind nucleotide activation since it was crystallized in the liganded (bound) and unliganded (unbound) states, fig. 4 [12,16]. The main difference between the bound and unbound states is the rearrangement of the helices [17]. In the bound state, PBC and helix αC collapse around the ligand protecting it from the solvent while in the unbound state these can occupy multiple positions. Particularly important for channels is the repositioning of the loop between αA' and αA since this movement is reflected on the position of αA' (C-linker) and is thought to lead to changes in the gate.

EAG channel inhibition by Ca^{2+}/calmodulin

Besides changes in the membrane electric field, EAG channels are also regulated by calmodulin. Elevation of intracellular calcium (Ca^{2+} half maximal inhibitory concentration, IC_{50}, of ~100 nM [18,19]) inhibits channel activity. This means that EAG channels undergo inhibition just above basal cytosolic Ca^{2+} concentrations. It has been shown that this Ca^{2+} sensitivity requires the calcium-binding protein calmodulin (CaM) since neither Ca^{2+} nor CaM alone are able to block EAG currents [19].

Three putative CaM binding regions were identified in a peptide array screen - one in the N-terminus (BD-N, between the PAS domain and S1) and two in the C-terminus (BD-C1 and BD-C2, just after the CNBD), fig. 5 [20]. Using fluorescence correlation spectroscopy and surface plasma resonance spectroscopy the following dissociation constants were estimated: 150-180 nM for BD-N and 130-200 nM for BD-C2. BD-C1 showed low affinity (from 300 nM to >5000 nM) or no binding at all to hCaM, depending

on the assay and fluorescent label used [20]. Although mutations in all three regions reduce the inhibition of EAG currents by Ca^{2+} [19,20], channels with both disrupted BD-N and BD-C2 no longer bind Ca^{2+}/CaM [21] which implies that BD-C1 is not able to bind CaM on its own but may do so in a cooperative manner. In general, mechanisms of regulation by CaM are not understood in many protein systems. In particular, the molecular mechanism behind EAG channel regulation by Ca^{2+}/CaM remains unclear mainly due to the lack of structural information on the cytosolic binding domains in complex with CaM.

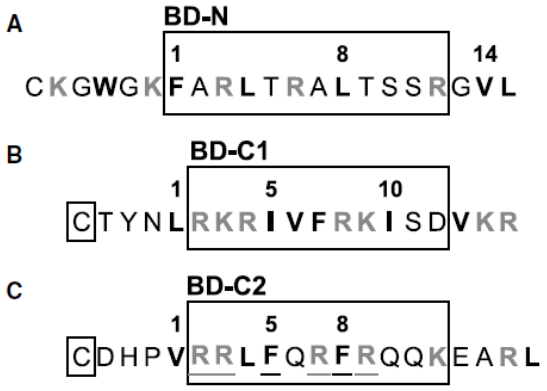

Fig. 5 - hEAG1 sequences identified as CaM binding sites. A - BD-N; B - BD-C1; C - BD-C2. Hydrophobic residues are in bold and basic residues in grey. Adapted from [20].

Aims of the project

EAG channels are voltage-gated potassium channels that are inhibited by Ca^{2+}/Calmodulin. These channels have a putative CNBD although they show no regulation by cyclic nucleotides nor bind these ligands. There are a lot of solved structures of CNBDs, including ones from a prokaryotic and eukaryotic cyclic nucleotide regulated channels, but there are none of the EAG potassium channel family. I wanted to solve a structure of an EAG CNBD to try to understand the structural features that make these domains not bind cyclic nucleotides.

Furthermore, I wanted to characterize the interaction of calmodulin with two putative calmodulin binding regions downstream of mEAG CNBD, determine the stoichiometry and see if a conformational change of the domain occurs upon binding of calmodulin.

Materials and Methods

Molecular biology

DNA constructs were produced using standard cloning techniques [22]. Inserts were amplified by 25 cycles of PCR using the Pfu polymerase (Fermentas). Both PCR product and expression vector were digested with the two chosen restriction enzymes (Table 1) for 3h at 37 ^{o}C. Digestion products were purified by electrophoresis on a 1% agarose gel and the DNA bands with the expected molecular weight were excised under UV_{254} light. The DNA was extracted from the excised pieces of agarose using a QIAGEN Gel Extraction Kit. Ligation reactions were routinely performed using three different ratios of purified PCR product:expression vector in the presence of T4 DNA ligase (Fermentas) for 1h at room temperature.

Table 1 - Description of the residue limits, oligonucleotides and restriction enzymes used to clone the constructs in the host vectors

Host expression vector	**Residue limits of construct**	**Restriction enzymes**	**Oligonucleotides (5'→3')** (F: forward; R: reverse)
pRSFDuet-1 (MCS1*/MCS2) (Novagen) kan^{r} *thrombin cleavage site was added after BamHI to allow excision of His-tag	mEAG 503-724/-	BamHI+NotI	F-ccggatccgctggtgccgcgcggcagccagcagatg R-tacgccccctttaagcggccgcctactacttccgtttcatcc
	mEAG 552-724/-	BamHI+NotI	F-cccggatccgctggtgccgcgcggcagcacagagaaggtcctgc R-tacgccccctttaagcggccgcctactacttccgtttcatcc
	mEAG 552-724/hCaM full length	BamHI+NotI/ NdeI+XhoI	F-cccggatccgctggtgccgcgcggcagcacagagaaggtcctgc R-tacgccccctttaagcggccgcctactacttccgtttcatcc / F-gccatatggctgatcaactgacagaag R-gcgctcgagctacttcgctgtcatcatctgtac
	mEAG 552-757/hCaM full length	BamHI+NotI/ NdeI+XhoI	F-cccggatccgctggtgccgcgcggcagcacagagaaggtcctgc R-ccgctcgagctactaccctctctcggctgc / F-gccatatggctgatcaactgacagaag R-gcgctcgagctacttcgctgtcatcatctgtac
pET-15b (Novagen) amp^{r}	mEAG 552-707	NdeI+XhoI	F-cccggatccgctggtgccgcgcggcagcacagagaaggtcctgc R-ccgctcgagctactagaacacaatcctcttcctcag
	mEAG 562-707	NdeI+XhoI	F-ggaattccatatggacatgcgagccgac R-ccgctcgagctactagaacacaatcctcttcctcag
	mEAG 552-757	NdeI+XhoI	F-cccggatccgctggtgccgcgcggcagcacagagaaggtcctgc R-ccgctcgagctactagaacacaatcctcttcctcag

Note - after thrombin cleavage of the His-tag the protein fragment has the extra residues GS (pET-15b) or GSHM (pRSF Duet-1).

Ligations were transformed [22] into competent dH5α cells and plated onto LB agar plates with the appropriate antibiotic (50 mg/L kanamycin or 100 mg/L ampicillin). The following day colonies were picked and inoculated into LB liquid media+antibiotic. Cultures were grown overnight and positive clones were accessed by PCR with the respective forward and reverse oligonucleotides. DNA was prepared from these cultures using a miniprep kit and sequenced.

Recombinant protein expression and purification - mEAG

Protein expression followed a standard protocol: BL21(DE3) competent cells were transformed with expression vector and then plated on LB agar+antibiotic; the following day resuspended colonies were grown in liquid LB+antibiotic at 37 °C, 160 rpm until they reached an OD_{600} between 0.6-0.8. At that point cultures were put in an ice bath for 30 min (induction of cold shock chaperones), after which ethanol was added slowly to a final concentration of 2% (induction of heat shock chaperones), and 0.5 mM IPTG was added for an overnight induction at 18 °C (12-16h).

Cultures were harvested by centrifugation at 5000 rpm, 20 min, 4 °C (Beckman rotor JLA 8-1000) and the resulting pellet was either stored at -20 °C or immediately resuspended in lysis buffer (table 2 for buffer description) supplemented with the protease inhibitors PMSF (1 mM), leupeptin (1 µg/mL) and pepstatin (1 µg/mL). Cell lysis was done in a cooled cell cracker (Emulsiflex-C5, AVESTIN) subjecting the lysate to three cycles at ~15000 psi. The lysate was then centrifuged at 20000 rpm (Beckman rotor JA-25.50) for 45 min at 4 °C to remove cell debris. Purification was done in two steps, immobilized metal affinity chromatography (IMAC) followed by size-exclusion chromatography. Samples of each purification step were kept for SDS-PAGE analysis. In more detail, the supernatant from centrifugation was loaded onto TALON Cobalt beads (Clontech) pre-equilibrated with lysis buffer and three washes (W0+1+2) were made before eluting the His-tagged protein with elution buffer.

Table 2 - Buffers used during purification

	Tris HCl pH 8.0 (mM)	NaCl (mM)	Imidazole (mM)	DTT (mM)	$CaCl_2$ [c] (mM)
Lysis buffer (W0)	50 [a]	150	0	0	1
			5 [b]		
Wash buffer 1 (W1)	50 [a]	150	5	0	
		300 [b]	0 [b]		
Wash buffer 2 (W2)	50 [a]	150	20	0	
Elution buffer (E)	50 [a]	150	150	0	
Gel filtration buffer	50 [a]	150	0	5	

[a] - 20 mM Tris HCl was used for crystallization trials.
[b] - Buffers were used with constructs pET-15b mEAG552-757, pRSF Duet-1 mEAG 552-724/hCaM full length and pRSF Duet-1 mEAG 552-757/hCaM full length, in an attempt to increase purity.
[c] - 1 mM $CaCl_2$ was added when purifying mEAG co-expressed with hCaM.

Eluted protein, in the presence of thrombin to cleave the tag, was dialysed overnight at 4 °C against gel filtration buffer (volume ratio 1:~150) to remove excess imidazole using Spectra/Por membranes with molecular weight cutoff of 10000 Da. The dialysed non-tagged protein was concentrated in Vivaspin concentrators (Vivascience) with 10000 Da cutoff; the filtrate was passed through a 0.22 μm filter to remove particles. Further purification was achieved by 300-500 μL injections into a pre-equilibrated gel filtration Superdex 200 column (Pharmacia).

Protein purity was evaluated by SDS-PAGE (15% Laemli [22]). Protein concentration was determined by measuring absorbance at 280 nm in an Ultrospec plus spectrophotometer (Pharmacia), using the calculated extinction coefficients obtained from ProtParam, a tool available at ExPaSy web server, http://www.expasy.org/tools/protparam.html (Table 3).

Table 3 - Protein absorbances at 280 nm calculated by Protparam tool

	OD_{280} (at 1 mg/mL)	**ε (M^{-1} cm^{-1})**
mEAG 503-724	0.880	22920
mEAG 552-724	0.567	11460
mEAG 562-707	0.691	11460
mEAG 552-707	0.637	11460
mEAG 552-757	0.443	11460

Recombinant protein expression and purification - hCaM

BL21(DE3) competent cells were transformed with expression vector (pT7-7 hCaM) and then plated on LB agar+ampicillin; the following day resuspended colonies were grown in liquid LB+ampicillin at 37 °C, 160 rpm until they reached an OD_{600} between 0.6-0.8. 0.5 mM IPTG was added followed by a 3h induction at 37 °C.

Cultures were harvested by centrifugation at 5000 rpm, 20 min, 4 °C (Beckman rotor JLA 8-1000) and the resulting pellet was either stored at -20 °C or immediately resuspended in lysis buffer (table 4 for buffer description) supplemented with the protease inhibitors PMSF (1 mM), leupeptin (1 µg/mL) and pepstatin (1 µg/mL). Cell lysis was done in a cooled cell cracker (Emulsiflex-C5, AVESTIN) subjecting the lysate to 3 cycles at ~15000 psi. The lysate was then centrifuged at 20000 rpm (Beckman rotor JA-25.50) for 45 min at 4 °C to remove cell debris. Supernatant was loaded onto a Phenyl Sepharose CL-4B (Sigma-Aldrich) column equilibrated in EDTA buffer to absorb proteins that bind in a calcium-independent manner. The flow-through that contains CaM was collected and $CaCl_2$ was added to a final concentration of 5 mM. The calcium supplemented flow-through was loaded onto another phenyl sepharose column equilibrated in calcium buffer. This second step allows CaM to interact with the phenyl sepharose matrix since there is calcium available. Washes were made with calcium buffer + NaCl and calcium buffer. Calmodulin was eluted with EDTA buffer. Protein purity was evaluated by SDS-PAGE and concentration was determined by measuring absorbance at 277 nm (calmodulin does not have any tryptophans in the sequence) in an Ultrospec plus spectrophotometer (Pharmacia), using the extinction coefficient ε_{277}=3029 M^{-1} cm^{-1} [23]. Calmodulin was dialyzed against storage buffer using a dialysis membrane with 3500 Da cutoff and stored at -80 °C.

Table 4 - Buffers used for CaM purification

	Tris HCl pH 7.5 (mM)	NaCl (mM)	EDTA (mM)	DTT (mM)	$CaCl_2$ (mM)	NaN_3 (mM)
Lysis buffer (EDTA buffer + NaCl)	50	100	2	5	0	0
EDTA buffer	50	0	2	5	0	0
Calcium buffer	50	0	0	5	1	0
Calcium buffer + NaCl	50	100	0	5	1	0
Storage buffer	2	0	0	2	0	1

Crystallography

Crystallization trials were performed using the vapour diffusion method [24]. Pure protein was concentrated up to 10 mg/mL in 20 mM Tris HCl pH 8, 150 mM NaCl, 5 mM DTT and centrifuged at 14000 rpm for 30 min in a refrigerated table-top centrifuge to remove particles before setting plates.

The following commercial random crystallization screens were used: Nextal Tubes Classics Suite, Nextal Tubes Classics II Suite, Nextal Tubes Classics L Suite, MBClass Suite (QIAGEN); Wizard I+II, Precipitant Synergy P64 (Emerald Biosystems); Crystal Screen I+II, MembFac (Hampton Research). 96-well sitting drop plates were set at 4 and 20 °C using a drop with 1 µL:1 µL mixture of precipitant solution to protein solution and 100 µL of commercial solution in the reservoir. When crystals showed up, fine screens around the hit condition were prepared by varying pH, precipitant concentration, ionic strength and ratio between precipitant solution and protein solution and set in 24-well plates with 300 µL of precipitant solution in the reservoir.

Microseeding was necessary to reproduce some crystals [25,26]. A crystal was picked, washed and diluted in a solution with higher precipitant concentration and then crushed into very small pieces. With the help of a 0.05 mm cryoloop, several micro crystals were transferred into freshly set drops. Volume ratios of protein:precipitant of 3:1, 2:1 and 1:1 were also tried to further optimize crystal growth.

Cryoprotectant solutions were prepared by supplementing the crystallization solution with cryoprotectant agent - PEG 400 or glycerol - generally in 5% steps [27,28]. The solutions that showed vitrification in the crystal loop when exposed to a stream of N_2 vapour at 100 K were selected. Crystals were prepared for data collection by fast equilibration in several intermediate solutions, ending in the final cryoprotectant solution and flash frozen in liquid nitrogen.

Data collection and refinement

A complete dataset was collected at the ID14-4 beamline of the European Synchrotron Radiation Facility (ESRF). Data were integrated using the program Mosflm and scaled using SCALA, both from Collaborative Computational Project 4 (CCP4) [29]. Initial phases were calculated by molecular replacement using Phaser (CCP4). Model refinement was done in Refmac5 (CCP4) and in the final stages of refinements Phenix [30] was used, together with TLS parameters [31]. Model building was performed in Coot [32] and figures were made using Pymol 1.2r2 (www.pymol.org).

Controlled and *in situ* proteolysis for protein crystallization

Pre-screenings to identify ideal proteases were performed with four proteases - trypsin (Worthington Biochemical Corporation), chymotrypsin (Worthington Biochemical Corporation), Lys-C (Roche) and Glu-C (Roche). Stock solutions of protease were serially diluted into a buffer comprising 10 mM HEPES pH 7.5 and 500 mM NaCl [33,34]. 15 µg of protein, in gel filtration buffer, were digested with each protease for 1h at room temperature using the following mass ratios of protease:protein - 1:50, 1:100, 1:500, 1:1000. Digestions were interrupted by addition of SDS sample buffer (62.5 mM Tris HCl pH 6.8; 25% glycerol; 2% SDS; 0.01% Bromophenol Blue; 0.7 M β-mercaptoethanol). Samples were analysed by SDS-PAGE. Proteases and ratios who gave rise to the larger cleavage products were further optimized by varying times of incubation from 45 min to 1h15min. These reactions were stopped with 0.1% formic acid and sent for mass

spectrometry analysis with 4700 MALDI TOF/TOF Proteomics Analyzer (Applied Biosystems) for identification of fragment masses.

The best conditions (combination of protease and reaction time) were also used for *in situ* proteolysis. Two strategies were applied: 1) protease at the chosen ratio was mixed with the protein for 1h at room temperature. Reaction was then stopped with an appropriate protease inhibitor and crystallization plates were set. 2) protease was added to the protein on ice just before setting plates. The reaction was not stopped [33,34].

Cross-linking between mEAG 552-757 and CaM

Molar ratios of 1:2, 1:5, 1:10 of mEAG 552-757 (2 µM) and CaM were incubated in 20 mM HEPES pH 7.5, 150 mM NaCl, 1 mM EDTA in the presence and absence of 5 mM $CaCl_2$ for 30 min at room temperature. Stock solutions of bifunctional primary amine cross-linkers (EGS spacer arm: 16 Å and DTSSP spacer arm: 12 Å) were prepared in 100% DMSO or in 5 mM citrate pH 5.5, respectively. Cross-linker was added to a final concentration between 0.5-2 mM and the reaction took place for 1 h at room temperature after which it was stopped by addition 50 mM Tris HCl pH 8 (final concentration). Samples were precipitated with tricloroacetic acid (TCA): Ice cold TCA 100% was added to the samples to a final concentration of 16.6%. Samples were incubated on ice for 30 min followed by a 30 min centrifugation at top speed in a refrigerated table-top centrifuge. The supernatant was carefully removed and dry acetone was added to the pellet followed by 15 min incubation in ice. The samples were centrifuged at top speed, 4 °C, the supernatant was removed and the pellets were air dried before adding sample buffer and analyzing by SDS-PAGE.

Derivatization of calmodulin with the fluorophore Dansyl-Cl

Wild-type hCaM was derivatized with 5-(dimethylamino)naphthalene-1-sulfonyl chloride (Dansyl-Cl, Molecular Probes), a reagent that reacts with primary amines, as described in [35,36]. Briefly, CaM was diluted to 1 mg/mL in 20 mM sodium bicarbonate pH 10, 100 mM NaCl, 250 µM $CaCl_2$. Dansyl-Cl was diluted to 1 mg/mL in dry acetone and 1.5

moles dansyl-Cl were added per mol of CaM. The reaction took place in the dark, at room temperature, for 60-90 min after which it was stopped with 50 mM Tris HCl pH 8. Excess dye was removed using a size exclusion Sephadex G25 column (Pharmacia) and buffer was exchanged to 20 mM Tris HCl pH 8, 150 mM NaCl. Dansyl-CaM was kept at 4 °C in the dark. The amount of dansyl incorporated was estimated by determination of absorbance at 334 nm (λ_{max} bound dansyl, ε_{334}=3400 cm^{-1} M^{-1}) and related to protein concentration to give moles dansyl/mol CaM.

Fluorescence assay - binding of Dansyl-CaM to mEAG 552-757

Dansyl-CaM at 40 nM was incubated with different concentrations of protein at room temperature, for at least 20 min, in 50 mM Tris HCl pH 8, 150 mM NaCl, 5 mM $MgCl_2$, 0.1 mM EGTA and 2 mM $CaCl_2$ (1.9 mM free Ca^{2+}). Fluorescent measurements were made at 26 °C using a Horiba Fluoromax-4 spectrofluorimeter. All emission spectra were obtained using an excitation wavelength of 340 nm, with slit widths of 6 nm [36].

Results and Discussion

Calibration of Superdex 200 column

To be able to translate size-exclusion column elution volumes (Ve) into approximate molecular weights, the Superdex 200 column used for purification of all protein constructs was calibrated using a protein standard kit (Sigma) The standards used were blue dextran (MW=2000 kDa, corresponding to the void volume of the column, V0), apoferritin (MW=443 kDa), β-amylase (MW=200 kDa), ADH (MW=150 kDa), BSA (MW=66 kDa) and myoglobin (MW=16.7 kDa). The log MW was ploted against Kav (Kav=$\frac{Ve-V0}{Vt-V0}$ in which Vt is the total bed volume 24 mL) and a line was fitted to the points, fig. 6.

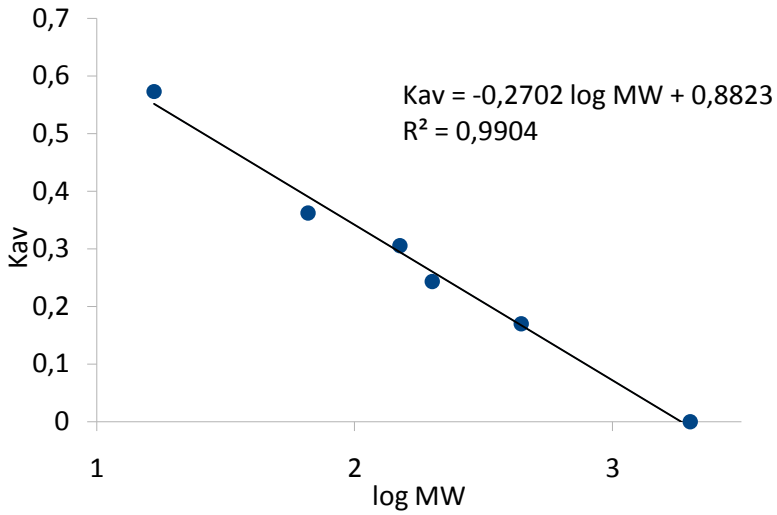

Fig. 6 - Calibration curve of Superdex 200 size-exclusion column

mEAG 503-724

The first construct tested - mEAG 503-724 - included the complete C-linker, αA'-αF', and extended about 20 residues after the CNBD, after BD-C1 (see Appendix 1). This protein was very sensitive to proteolysis; the protein also precipitated heavily during elution from the His-tag affinity beads and did not have a monodisperse size-exclusion profile. For all the problems cited above mEAG 503-724 was abandoned.

mEAG 552-724

mEAG 552-724 starts at the beginning of helix αC' of the C-linker and results in a protein with a molecular weight of 19926 Da after excision of the His-tag. This truncation is soluble and gives a yield of 10-20 mg pure protein/L of culture. In size-exclusion chromatography it is eluted as a species of 20 kDa which is very close to the actual molecular weight of the protein, fig. 7. Extensive random crystallization screening of mEAG 552-724 did not result in any hits.

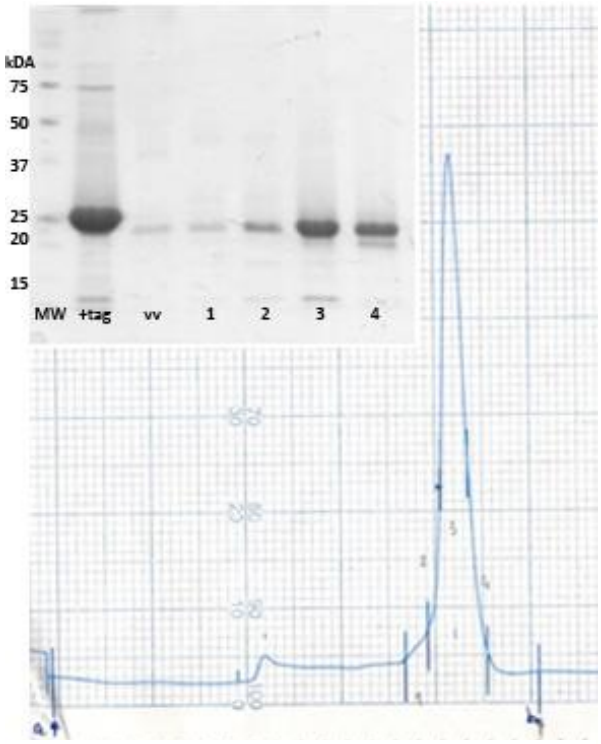

Fig. 7 - Gel filtration profile and SDS-PAGE analysis of mEAG 552-724. MW - molecular weight markers; + tag - protein before thrombin cleavage; vv- void volume; 1-4 - fractions of the peak. Arrow indicates the sample injection. Chart speed 0.5 cm/mL. The molecular weight markers are the same for all the gels.

Controlled proteolysis / *In situ* proteolysis

mEAG 552-724 was then used in controlled proteolysis trials. This technique is useful for defining a protein core that is partially resistant to proteases, and which will potentially crystallize more easily and yield better diffracting crystals [33,34].

Of the four proteases originally tested, trypsin produced fragments that were too small and Glu-C hardly cleaved the protein at all, even at high concentrations, fig. 8 and 9. Digestions with chymotrypsin at 1:500 and Lys-C at 1:100 (protease:protein mass ratio) originated species with a molecular weight corresponding to removal of small portions of the protein termini; these conditions were further optimized by varying time of digestion (fig. 10). The proteolysis products of the chymotrypsin and Glu-C after 1h digestion were

sent for mass determination of the fragments by mass spectrometry. Data analysis was performed using the software Paws (Genomic Solutions Inc.). The chymotrypsin (1:500)

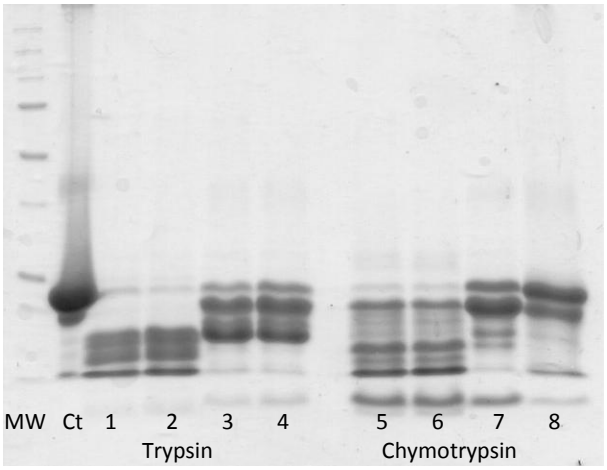

Fig. 8 - SDS-PAGE analysis of trypsin (T) and chymotrypsin (C) digestion products (1 h at room temperature). Ct - control undigested protein; 1 - T 1:50; 2 - T 1:100; 3 - T 1:500; 4 - T 1:1000; 5 - C 1:50; 6 - C 1:100; 7 - C 1:500; 8 - C 1:1000

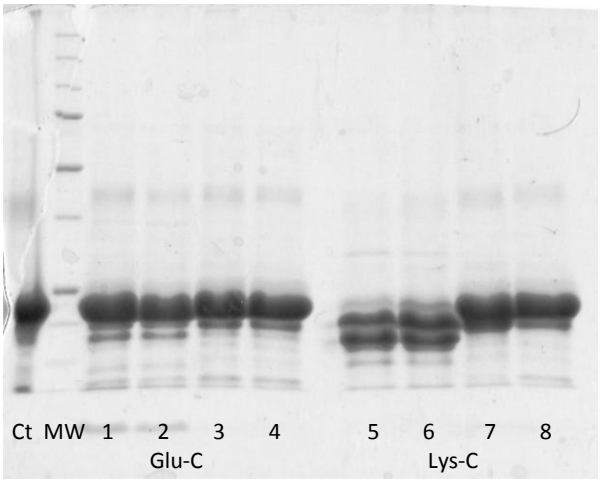

Fig. 9 - SDS-PAGE analysis of Glu-C (G) and Lys-C (L) digestion products (1 h at room temperature). Ct - control undigested protein; 1 - G 1:50; 2 - G 1:100; 3 - G 1:500; 4 - G 1:1000; 5 - L 1:50; 6 - L 1:100; 7 - L 1:500; 8 - L 1:1000

digestion gave rise to a species of 17726.9 Da corresponding most likely to mEAG 552-707 and the Lys-C (1:100) digestion originated a species of 16728.2 Da that corresponds to

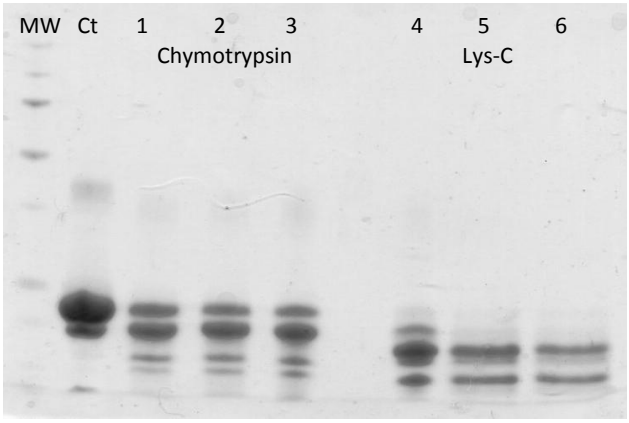

Fig. 10 - SDS-PAGE analysis of chymotrypsin (C) 1:500 and Lys-C (L) 1:100 digestion products (at room temperature). Ct - control undigested protein; 1 - C 45min; 2 - C 1h; 3 - C 1h15; 4 - L 45min; 5 - L 1h; 6 - L 1h15

mEAG 562-709, see spectra in Appendix IV. The residues Thr552, Asp562 and Phe707 correspond to the beginning of the helix αC', helix αD' and a few residues after the end of helix αC, respectively (see MSA, Appendix I).

In situ proteolysis consists of the addition of trace amounts of protease to crystallization trials without stopping the reaction. This has proven to be a successful

crystallization technique for proteins that had previously failed in crystallization trials and structure determination [33,34]. *In situ* proteolysis crystallization trials of mEAG 552-724 in the presence of chymotrypsin 1:500 or Lys-C 1:100 did not yield any hits.

mEAG 562-707

Based on the controlled proteolysis results two new constructs were designed: mEAG 562-707 and 552-707. After expression and purification of both protein fragments crystallization trials were performed. During purification of mEAG 562-707, precipitation was detected in the dialysis and concentration steps. The size-exclusion profile was

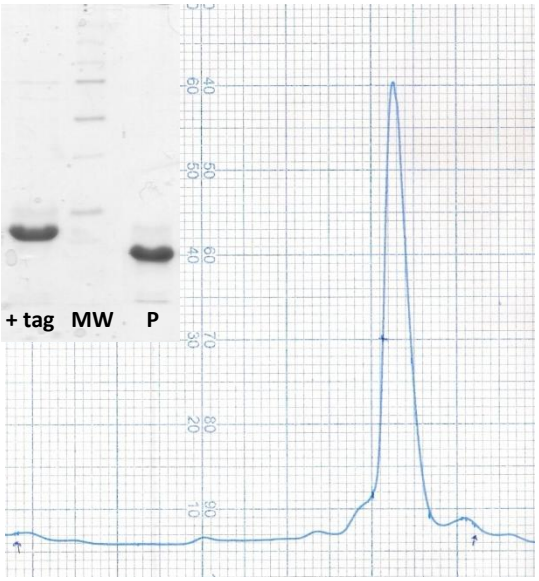

Fig. 11 - Gel filtration profile and SDS-PAGE analysis of mEAG 562-707. MW - molecular weight markers; + tag - protein before thrombin cleavage; P - centre of peak. Arrow indicates the sample injection. Chart speed 0.5 cm/mL.

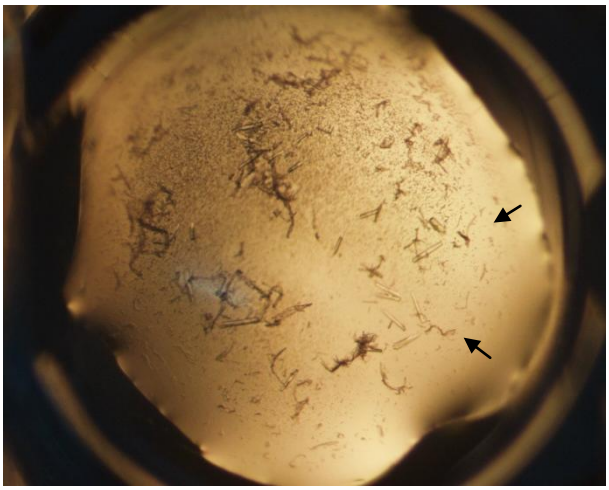

Fig. 12 - Needle-like crystals of mEAG 562-707 at 12 mg/mL in 0.05 M ammonium sulphate, 0.05 M bis-tris HCl pH 6.5 and 30% (v/v) pentaerythritol ethoxylate (15/4 EO/OH) at 4 °C.

monodisperse, did not have a significant amount of aggregated protein, and the protein migrated as a species of approximately 14 kDa (fig. 11).

Random screen crystallization plates were set and needle-looking crystals were obtained with Nextal Classics II condition 57: 0.05 M ammonium sulphate, 0.05 M bis-tris HCl pH 6.5 and 30% (v/v) pentaerythritol ethoxylate (15/4 EO/OH) at 4 °C, fig. 12. Fine screens around that condition were prepared but crystals were never obtained.

Subsequent protein preparations showed intense precipitation. For all this, it was decided not to pursue this protein any further.

mEAG 552-707

In contrast to the smaller construct, mEAG 552-707 did not precipitate. The expected molecular weight of the protein is 17995 Da and it migrated in size-exclusion as a 16 kDa species fig. 13. Random crystallization screens resulted in a hit. Condition 97 of Nextal Classics II - 0.2 M tri-sodium citrate dihydrate, 20% PEG 3350 - showed a single cluster of well defined crystals and multiple spherolites at 4 °C (fig. 14). Fine screens around the condition did not reproduce the crystals of mEAG 552-707. However, microseeding proved to be the solution for obtaining new crystals, fig. 15. The concentration of precipitant was lowered to the range of 8-18% PEG 3350 in order to

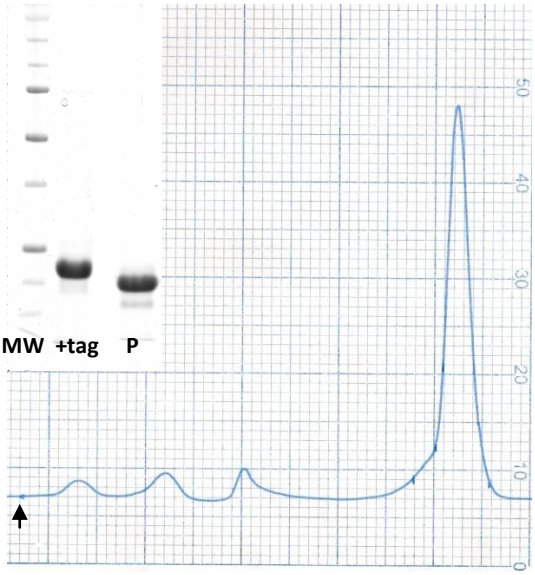

Fig. 13 - Gel filtration profile and SDS-PAGE analysis of mEAG 552-707. MW - molecular weight markers; + tag - protein before thrombin cleavage; P - centre of peak. Arrow indicates the sample injection. Chart speed 0.5 cm/mL.

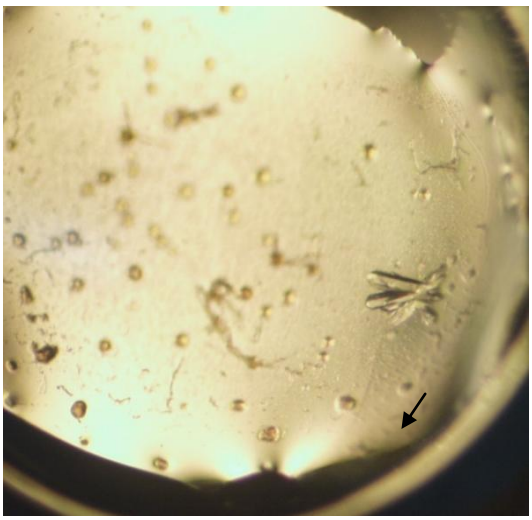

Fig. 14 - Crystals of mEAG 552-707 12 mg/mL in 0.2 M tri-sodium citrate dihydrate, 20% PEG 3350 at 4 °C are indicated by an arrow.

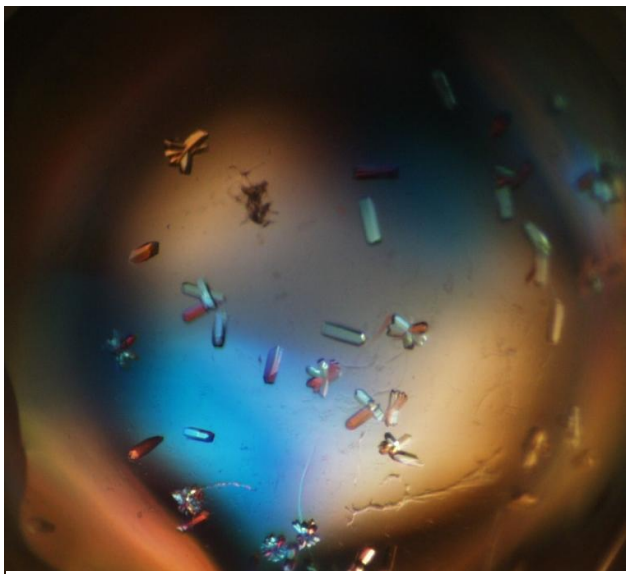

Fig. 15 - Crystals of mEAG 552-707 obtained by microseeding.

improve the quality of the crystals, otherwise they grew too fast and formed small and imperfect clusters. The crystals were flash-frozen on a cryoprotectant solution containing 25% PEG 3350, 0.2 M tri-sodium citrate and 10% glycerol.

Data collection

Two data sets were collected at 100 K from a single crystal of mEAG 552-707, comprising 270 images, 1° oscillation each, with a crystal-to-detector distance of 290 mm. To record the high-angle diffraction spots (at 2.2 Å, high resolution) the first data set was collected with a beam transmission of 100%. For the low-angle diffraction spots (low resolution), that were overloaded on the previous data set, another data set was collected with an attenuated beam (transmission of 10%).

From each data set, 90 images were indexed in space group $P3_121$ and integrated using Mosflm. Only 90 images were used because the crystal suffered radiation damage during data collection and lost diffraction quality. Mosflm suggested the spatial group (Table 4), but since this group has the same reflection conditions as $P3_221$ (000l:l=3n), it was only determined at a later stage. The integrated data (high and low resolution) were merged into one full data set and the statistics are shown on table 5.

Table 5 - mEAG 552-707 crystal data.

Crystal data	
Crystal system	Hexagonal
Space group	$P3_121$
Unit cell parameters	
a=b (Å)	60.3
c (Å)	85.4
α=β (°)	90
γ (°)	120
Data-collection details	
Diffraction source	ESRF beamline ID14_4
Wavelenght (Å)	0.9765

Detector	ADSC Quantum Q315r
Resolution range (Å)	52.3-2.2 (2.31-2.2)
No unique reflections	9566 (1356)
No measured reflections	39240 (17118)
Multiplicity	6.2 (5.2)
Completeness (%)	99.4 (97.5)
I/σI	4.8 (2.2)
R_{sym} (%)	8.9 (25.1)

Note - the values in parenthesis correspond to statistics of the highest resolution shell of data

The cell content analysis tool of CCP4 proposed one molecule per unit cell and 50% solvent. Molecular replacement was attempted with Phaser, using mHCN2 CNBD structure (PDB code 1Q3E) as a search model (23% identity with mEAG 552-707) but it failed. The next step was to submit mEAG 552-707 sequence to the protein structure prediction server Phyre [37]. The output that comes from this server is a set of ten models (.pdb files) based on the highest scoring alignments. From the top ten models, an ensemble of six search models was used in Phaser - models of mEAG 552-707 created from PDB codes 1Q3E, 1VP6, 2PTM, 1CX4, 1NE6 and 2PQQ. This strategy provided a well defined solution. The electron density maps calculated with this solution showed features that were not present in the search models, confirming the validity of the solution.

Model building and refinement

Model building was performed in Coot [32]. Refinement of the structure was made using the programs Refmac5 (CCP4) and Phenix [30]; TLS refinement (translation/libration/screw axis) [31] was applied to further lower R_{free} and R_{work} by dividing the model into ten groups as determined by the server (http://skuld.bmsc.washington.edu/~tlsmd). The model is currently in the final stages of refinement and validation with an R_{free}=22.6% and R_{work}=19.4%.

Analysis of structure

The structure of mEAG 552-707 shows a canonical CNBD fold consisting of helix αA followed by an antiparallel β-roll and two helices, αB and αC, fig. 16. αC is relatively short, only has two helical turns, and is followed by a 14-residue coil C-terminal region that lies on the surface of the β-roll. There are also three short helices at the N-terminus (fig. 16, αD', αE', αF'); these helices are part of the C-linker that connects the domain to the pore. There is no electron density for the first 14 residues of the protein.

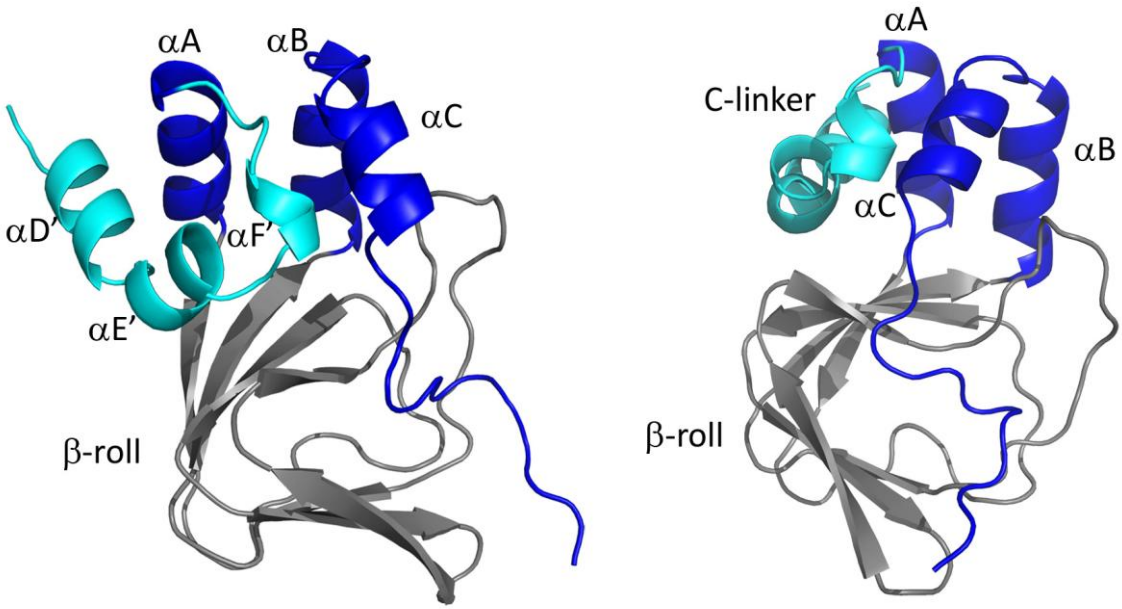

Fig. 16 - Two orientations of the mEAG 552-707 structure. CNBD helices are colored in blue, β-roll in grey and C-linker helices (αD', αE' and αF') in cyano.

One of the reasons to solve this structure was to understand why this domain does not bind cyclic nucleotides. No electron density corresponding to a cyclic nucleotide molecule could be identified in the ligand binding pocket of mEAG. Comparison of the binding pockets of the MlotiK liganded and unliganded structures with the equivalent region in the mEAG 552-707 structure shows that the residues close to the nucleotide base are unchanged (Val, Phe - fig. 17 in stick model); in contrast residues that in the MlotiK structure interact with the ribose and phosphate groups of the nucleotide are very different in the mEAG structure.

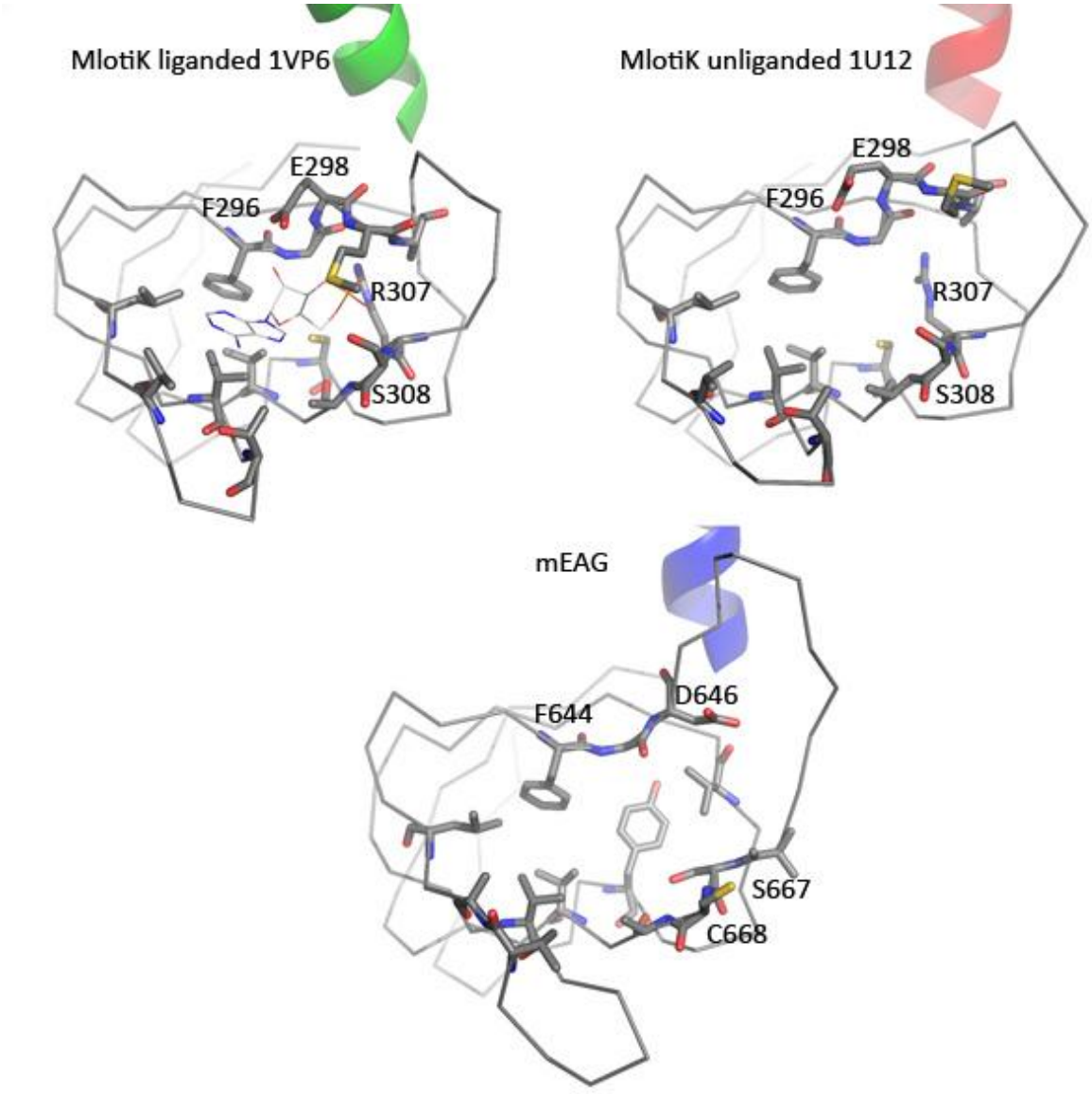

Fig. 17 - Close up of the nucleotide binding pocket in MlotiK liganded structure (1VP6 in green), in MlotiK unliganded structure (1U12 in red) and equivalent region in mEAG 552-707 (in blue). Residues of the PBC are labelled.

For instance, phosphate binding cassette (PBC) residues that are known to coordinate the ligand (Glu298, Arg307 and Ser308 in MlotiK - fig. 17 in sticks and labelled) are substituted in mEAG by residues with shorter side chains - Asp646, Ser667 and Cys668, respectively. Furthermore, the loop between β6 and β7 in mEAG has two extra residues relative to MlotiK and mHCN2, and it adopts a different conformation. This is particularly evident in the different position of the negatively charged residue of the PBC (Glu298 in MlotiK and Asp646 in mEAG). Overall the pocket of mEAG is wider than in either one of MlotiK structures (fig. 17); distances between the α-carbons of PBC's (Phe, Gly) and the residue across (Cys, in mEAG) are 2 Å larger than in the bound and unbound structures. There are four residues in the loop β6- β7 whose side chains were disordered and showed no electron density so they were mutated to Ala in the final model: Lys650Ala, Glu651Ala, Leu654Ala and Gln656Ala.

The mEAG domain structure was superposed with the two structures of MlotiK through the β-roll, a region that hardly varies among bound and unbound strutures (fig. 18). It has been demonstrated that the major change between liganded and unliganded states of CNBDs is the relative position of the helices. The position of the helices in mEAG

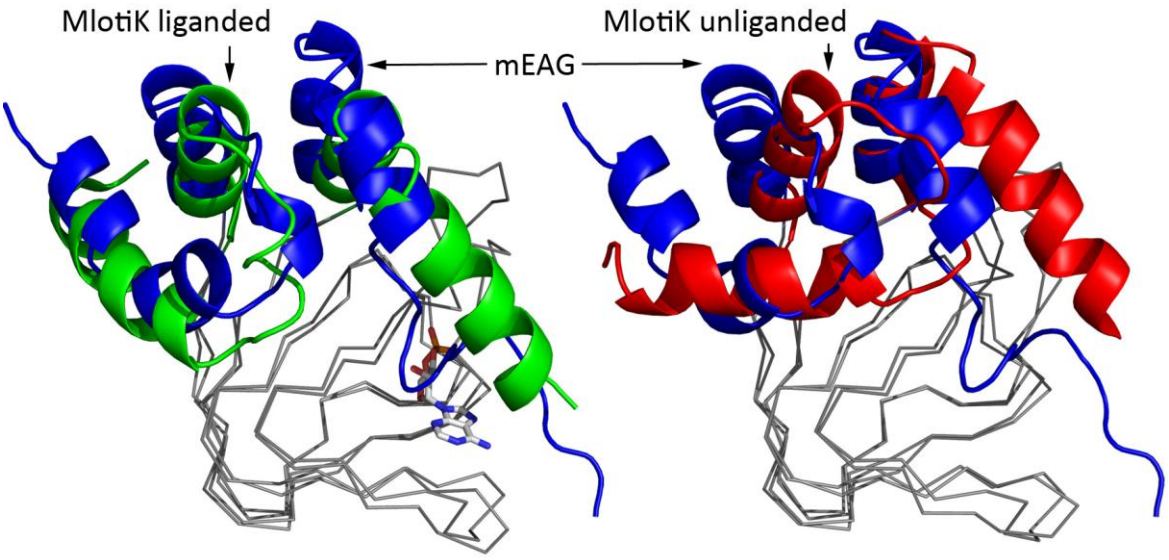

Fig. 18 - Superposition of mEAG (blue), liganded (1VP6, green) and unliganded (1U12, red) structures of MlotiK. β-rolls are represented in ribbon, cAMP of 1VP6 is in stick model.

structure is much more similar to the bound state of MlotiK, fig. 18. First of all, the αC-helix in mEAG aligns with the αC-helix of MlotiK bound state. Moreover, the region

formed by C-linker/loop/αA-helix in the mEAG structure basically occupies the same position on the surface of the β-roll as in the bound structure of MlotiK. Therefore, although there is no cyclic nucleotide in the ligand binding pocket of mEAG, it appears that it has adopted a bound state conformation. Strikingly, the C-terminal coil region that follows the αC-helix actually enters the binding pocket (fig.19); and the side chains of residues Tyr699 and Leu701 occupy the volume of the cAMP molecule in the bound structure of MlotiK (fig. 19, zoom in). The tyrosine ring lies on the same volume occupied by the nucleotide base and the leucine is positioned on the phosphoribose site.

These residues are fairly conserved among EAG channels, the tyrosine (consensus

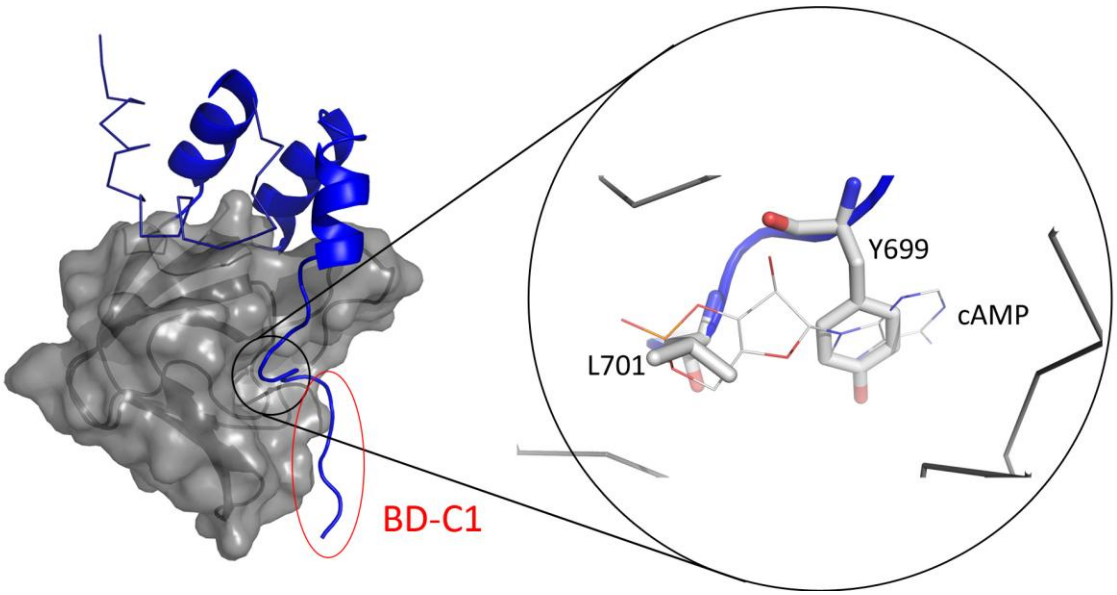

Fig. 19 - Surface view of the β-roll with C-terminal coil entering the pocket and zoom in on the residues (in sticks) that occupy the same space as cAMP (in lines), from MlotiK bound structure 1VP6.

of 46%) can be a phenylalanine (40%) or cysteine (14%) while the leucine (consensus of 96%) is sometimes substituted by isoleucine (4%). The observation of a bound state conformation, together with the positioning of Tyr699 and Leu701 in the binding pocket raises the possibility that, in the mEAG channel, the region immediately after the αC-helix may function as an internal ligand.

Immediately downstream from these residues there is a putative calmodulin binding site (BD-C1), fig. 19 and Appendix 1. This suggests a possible mechanism whereby

calmodulin modulates the switch between bound and unbound conformations of the CNBD and ultimately regulates the channel. Calmodulin binding to BD-C1 would shift the equilibrium between the bound and unbound conformations of the domain by stabilizing the conformation where the internal ligand is out of the pocket. This release of the internal ligand would induce a conformational change that is transmitted via C-linker to the pore, shutting it closed.

mEAG 552-724/ hCaM and mEAG 552-757 / hCaM - co-expression

The hypothesis raised above for calmodulin regulation lead us to propose four possible models for calmodulin binding. These models take in consideration that there are two putative calmodulin-binding sites after the domain, less than 30 residues apart from each other (fig. 20):

1) BD-C1 and BD-C2 bind CaM independently, one molecule in each site;
2) one CaM molecule wraps both CaM binding sites;
3) the two sites show cooperativity (CaM binding to one of the sites will change the affinity for the second);
4) BD-C1 was misidentified in the peptide screen and CaM only binds BD-C2.

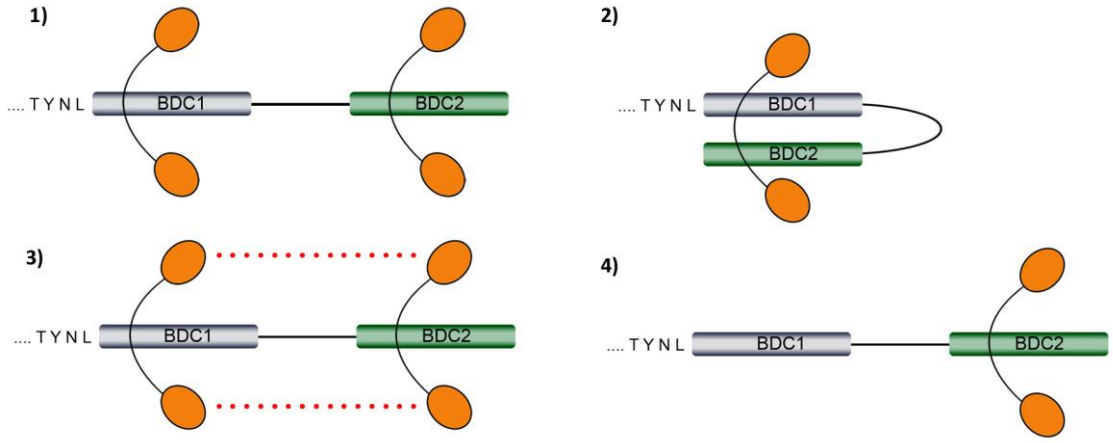

Fig. 20 - Scheme of the four proposed models for calmodulin binding. 1) two independent binding sites; 2) one CaM binds both sites; 3) there is cooperativity between both sites; 4) there is only one site (BD-C2). Calmodulin is represented in orange.

The models proposed above were tested by first checking if calmodulin binding depends on BD-C1. With that in mind two new constructs were designed and cloned into MCS1 of co-expression vector pRSF-Duet1: mEAG 552-724 only includes BD-C1; mEAG 552-757 contains both BD-C1 and BD-C2 and are His-tagged. On the MCS2 these constructs also encode and express untagged hCaM.

IMAC purification of mEAG 552-724 did not pull any calmodulin. Assembly of a complex between mEAG 552-724 and purified CaM was not detected by native gel analysis. These results are in accordance with published data that state that BD-C1 has low affinity to CaM and might not be able to bind CaM without BD-C2 [20,21].

Purification of mEAG 552-757 co-expressed with hCaM resulted in pulling down a complex between the two proteins, when the IMAC was performed in the presence of $CaCl_2$. The mEAG 552-757/CaM complex migrated in gel filtration as a 72 kDa species (fig. 21), considerably higher than mEAG 552-757 (~31 kDa species) or CaM (~25 kDa species) alone (fig. 23) and may correspond to an oligomeric form of mEAG 552-757/CaM.

To evaluate the complex and determine its stoichiometry it was necessary to prepare mEAG 552-757 without CaM. Since this protein expressed alone experienced severe proteolysis, a protocol had to be developed to separate mEAG 552-757 from CaM through a step of anion exchange chromatography in the presence of EDTA. The calculated isoelectric point (pI) of mEAG 552-757 and CaM are 8.9 and 4, respectively. Because of this difference in pI, these two proteins are easily separated in an anion exchange matrix at neutral pH.

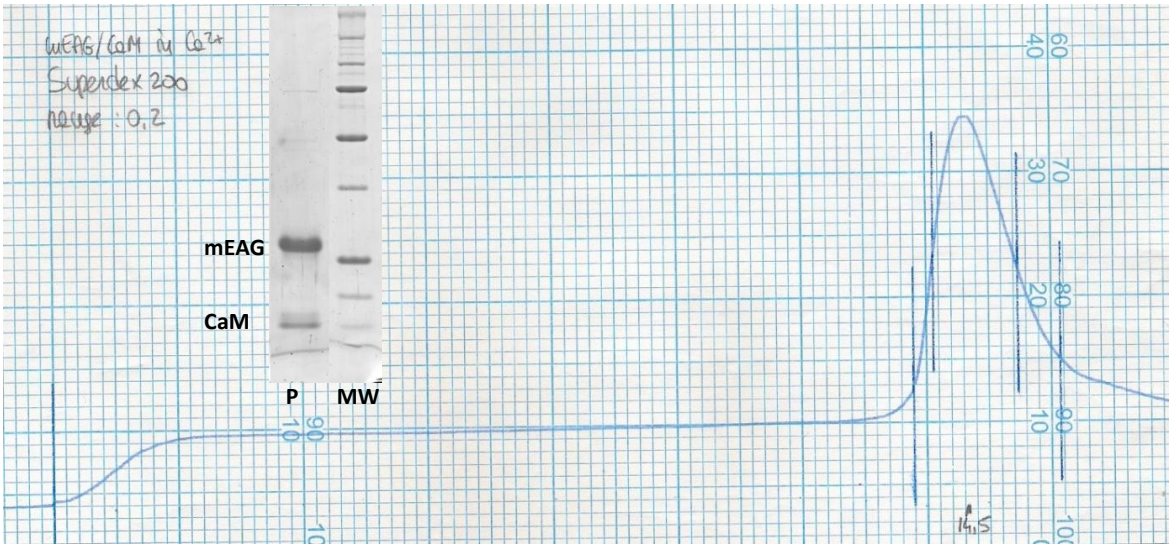

Fig. 21 - Gel filtration profile and SDS-PAGE analysis of mEAG 552-757. MW - molecular weight markers; P - centre of peak. Arrow indicates the sample injection. Chart speed 1 cm/mL.

Three approaches were used to begin the characterization of the complex between CaM and mEAG 552-757: gel filtration, cross-linking and a fluorescence binding assay.

Gel filtration profiles of the complex and chemical cross-linking

mEAG and CaM were incubated at ratio of 1:1 for 30 min on ice, in the presence of calcium, and analysed in a size exclusion column Superdex 200. A single peak of approximate molecular weight 72 kDa was observed, demonstrating that it is possible to reconstitute the complex formed in the bacteria (fig. 22). Formation of a complex in the

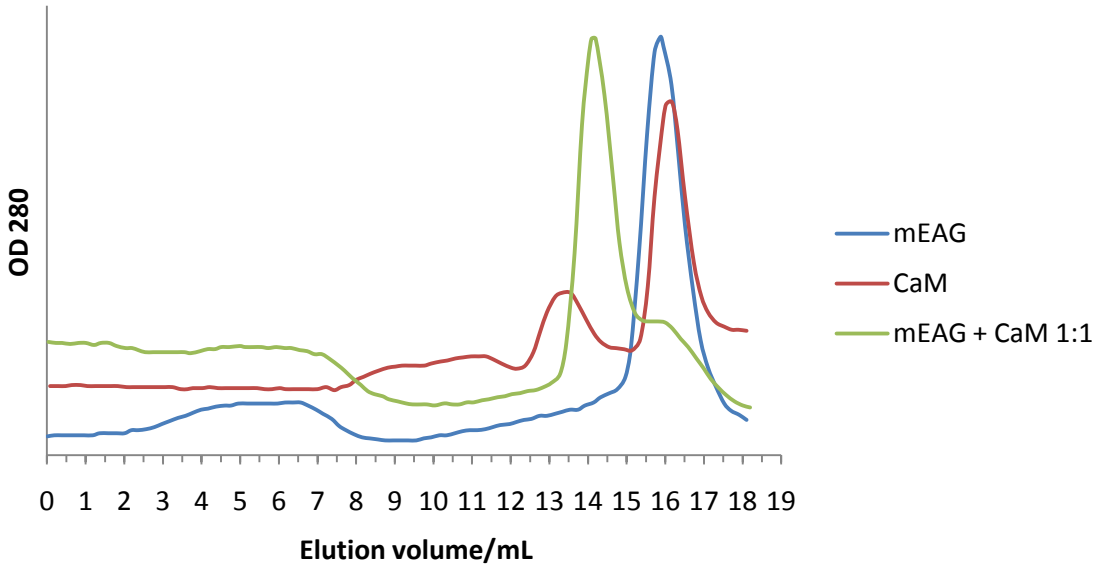

Fig. 22 - Superposition of gel filtration profiles of mEAG 552-757, CaM and 1:1 molar ratio of mEAG:CaM.

presence of a higher ratio of CaM (1:2), did not alter the migration of the 72 kDa species and showed the emergence of a peak at the elution volume of CaM (data not shown), hinting that CaM was in excess.

Chemical cross-linking of proteins allows the capture of transient interactions between proteins that might otherwise be hard to detect. Incubation of mEAG 552-757 with different molar ratios of CaM in the presence of cross-linking agents originated a single species, in a Ca^{2+}-dependent manner, with a molecular weight between 37 and 50 kDa, fig. 23. This species most probably corresponds to a 1:1 complex between CaM and mEAG 552-757 of expected molecular weight 43 kDa. Overall, the gel filtration and cross-linking experiments suggest that the complex between CaM and mEAG 552-757 involves one molecule of each protein.

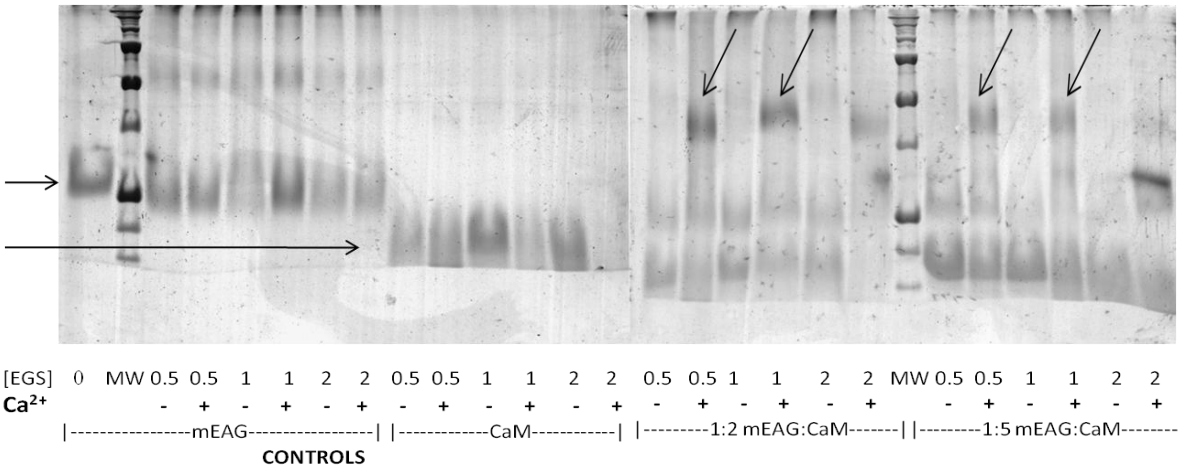

Fig. 23 - SDS-PAGE of cross-linking products. Controls are on the left and mixtures of mEAG and CaM on the right.

Fluorescent assay with dansyl-CaM

Previous reports of binding affinities of CaM to EAG calmodulin-binding sites have made use of small peptides [20]. To better understand the interaction between CaM and the mEAG C-terminal domain a fluorescence assay with dansyl-CaM was performed.

Dansyl-Cl is an environmental sensitive fluorophore. Dansyl-modified CaM retains the physical and biochemical properties of native CaM and has been used to monitor the formation of Ca^{2+}-dependent complexes with several calmodulin-binding proteins [36]. Apo dansyl-CaM (without calcium) shows an emission maximum at 520-525 nm. Upon

addition of Ca^{2+} the maximum shifts to ~505 nm and there is an increase in fluorescence intensity (data not shown). This Ca^{2+}-dependent blue shift results from a major conformational change that increases the hydrophobicity of the environment of the dansyl group increasing its quantum yield [36]. This blue shift and fluorescence intensity increase is further accentuated in the presence of a calmodulin ligand [36].

To assess if this assay could be applied to our protein system a test was performed, fig. 24. Three mixtures of dansyl-CaM and mEAG 552-757 were prepared either in the absence of Ca^{2+} (red); with 2 mM $CaCl_2$ (green) or with 2 mM $CaCl_2$ and 4 mM EGTA (blue) and fluorescence emission spectra were recorded. In the presence of Ca^{2+} there is an increase in fluorescence signal as well as a shift in the emission maximum from 514 nm to 483 nm that is almost completely reverted when excess EGTA is present. This result shows that the dansyl-CaM assay reports the formation of a Ca^{2+}-dependent complex between mEAG 552-757 and CaM.

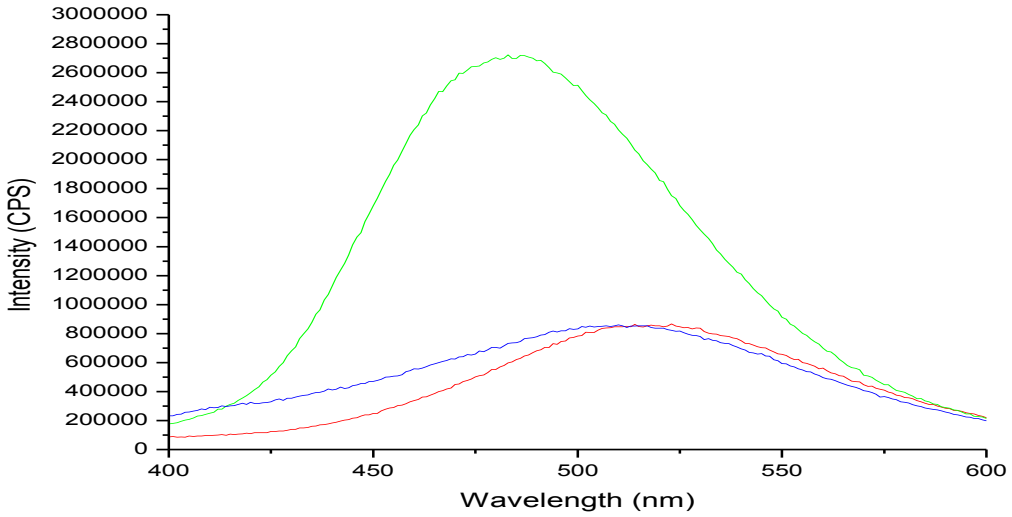

Fig. 24 - Emission spectra of 40 nM dansyl-CaM + 1 µM mEAG 552-757 with: no calcium (red); 2 mM $CaCl_2$ (green) and 2 mM $CaCl_2$ + 4 mM EGTA (blue).

Using this assay, a titration experiment was performed. Mixtures of 40 nM dansyl-CaM and increasing amounts of mEAG 552-757 were prepared and emission spectra were recorded. A progressive increase in fluorescence intensity, together with a blue shift of the emission maximum were observed with increasing mEAG 552-757, fig. 25, consistent with binding of mEAG to dansyl-CaM. The fluorescence intensities at this wavelength

were normalized using the formula $F\ norm = \frac{F-Fo}{Fmax-Fo}$ in which F norm is proportional to the concentration of [mEAG-Cam] complex. Averages and standard deviations of four titration experiments were calculated and plotted using OriginPro8.

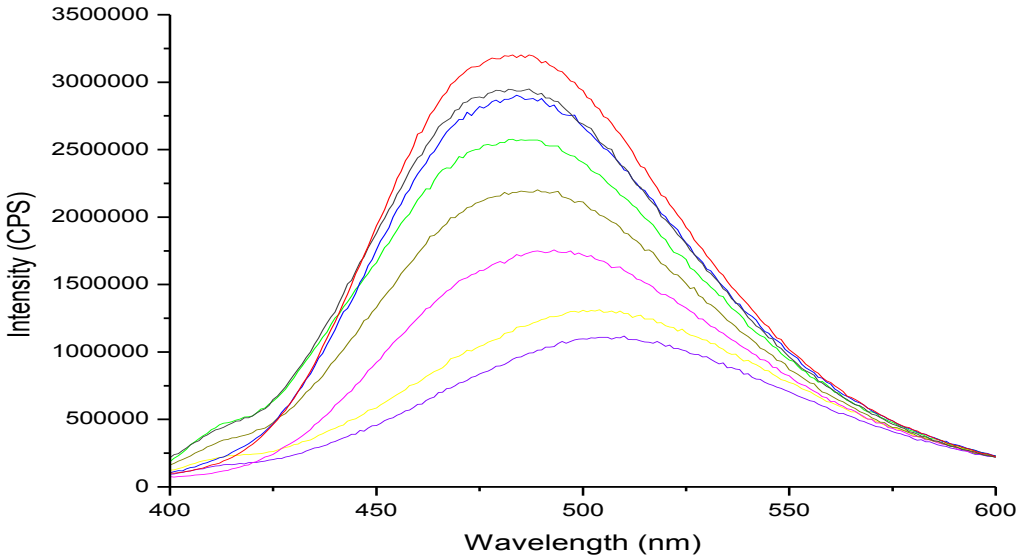

Fig. 25 - Emission spectra of 40 nM dansyl-CaM and increasing amounts of mEAG 552-757.

The normalized data were fitted to single-site binding model using the following hyperbolic function $Fnorm = \frac{[mEAG\ 552-757]}{Kd+[mEAG\ 552-757]}$. The determined K_d was 163 ± 18 nM (N=4), fig. 26, which compares very well to the previously determined affinity between CaM and the BD-C2 peptide [20]. Overall, these results suggest that only one molecule of calmodulin binds mEAG 552-757 and so far I have not been able to prove that BD-C1 is involved in CaM binding.

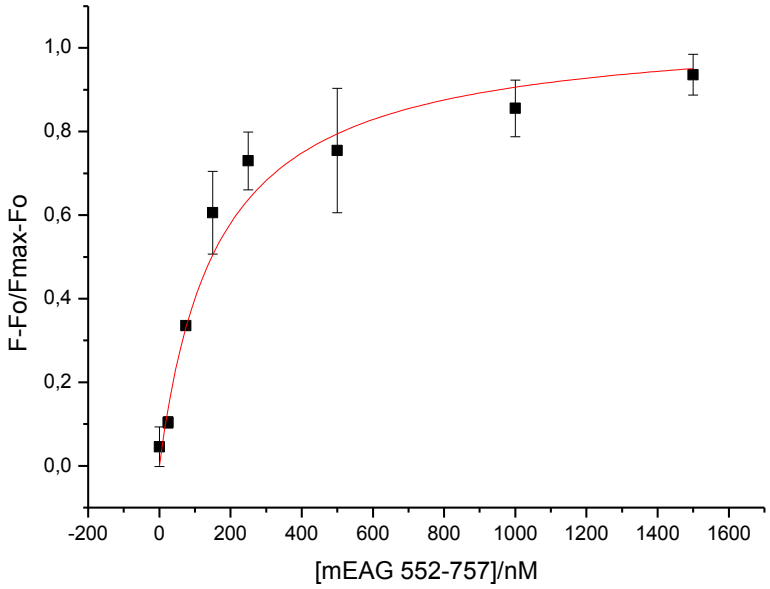

Fig. 26 - Data fitting to a hyperbolic function of four titration experiments.

Conclusions

A crystal structure of a putative CNBD from the EAG channel family was determined at a 2.2 Å resolution. The structure has the characteristic fold of cyclic nucleotide binding domains, and it appears to adopt a conformation that is equivalent to the bound state observed in CNBDs. Comparison between the binding pockets of CNBDs and the equivalent region in mEAG C-terminal domain show several important differences, consistent with the inability of mEAG to bind cyclic nucleotides.

The mEAG 552-707 structure shows a very interesting feature: two conserved residues in EAG channels reside in the volume occupied by the cAMP molecule in CNBD structures. Moreover, immediately after these residues there is a putative calmodulin binding site (BD-C1). These observations together with the bound state conformation of the mEAG domain structure have lead to the following hypothesis: a sequence of the C-terminal domain of the EAG channel acts as an internal ligand. Binding of CaM shifts the equilibrium towards a conformation this internal ligand is released from the binding pocket. This conformational change is transmitted to the pore region inhibiting the channel.

Future work

The hypothesis raised above requires further testing. For example, the importance of the internal ligand residues might be assessed by the functional impact of point-mutations in electrophysiological recordings in the presence and absence of Ca^{2+}-calmodulin.

Introduction of point-mutations in the different CaM binding sites, together with biochemical and structural analysis will provide a better picture of CaM binding and regulation.

Appendix I - Multiple sequence alignment of full-length mEAG (NP_034730.1), hEAG (NP_758872.1), hERG (NP_000229.1)**,** mHCN2 (NP_032252.1) and MlotiK (Q98GN8.1)

```
mEAG            MTMAGGRRGLVAPQNTFLENIVRRSNDTN--FVLGNAQIVDWPIVYSNDGFCKLSGYHRA 58
hEAG            MTMAGGRRGLVAPQNTFLENIVRRSNDTN--FVLGNAQIVDWPIVYSNDGFCKLSGYHRA 58
HERG            ---MPVRRGHVAPQNTFLDTIIRKFEGQSRKFIIANARVENCAVIYCNDGFCELCGYSRA 57
mHCN2           ---MDARGGGGRPGDSPGTTPAPGPPPPP---PPPAPPQPQPPPAPPPNPTTPSHPESAD 54
MlotiK          ------------------------------------------------------------

                                    PAS DOMAIN
mEAG            EVMQKSSACSFMYGELTDKDTVEKVRQTFENYEMNSFEILMYKKNRTPVWFFVKIAPIRN 118
hEAG            EVMQKSSTCSFMYGELTDKDTIEKVRQTFENYEMNSFEILMYKKNRTPVWFFVKIAPIRN 118
HERG            EVMQRPCTCDFLHGPRTQRRAAAQIAQALLGAEERKVEIAFYRKDGSCFLCLVDVVPVKN 117
mHCN2           EPGPRARLCSRDSACTPGAAKGGANGECGRGEPQCSPEGPARGPKVSFSCRGAASGPSAA 114
MlotiK          ------------------------------------------------------------

mEAG            EQDKVVLFLCTFSDITAFKQP-------------------------------------- 139
hEAG            EQDKVVLFLCTFSDITAFKQP-------------------------------------- 139
HERG            EDGAVIMFILNFEVVMEKDMVGSPAHDTNHRGPPTSWLAPGRAKTFRLKLPALLALTARE 177
mHCN2           EEAG------------------------------------------------------- 118
MlotiK          ------------------------------------------------------------

mEAG            ---------------------------------------IEDDSCKGWG---------- 149
hEAG            ---------------------------------------IEDDSCKGWG---------- 149
HERG            SSVRSGGAGGAGAPGAVVVDVDLTPAAPSSESLALDEVTAMDNHVAGLGPAEERRALVGP 237
mHCN2           ---------------------------------------SEEAGPA--G---------- 126
MlotiK          ------------------------------------------------------------

mEAG            ------------------------------------------------------------
hEAG            ------------------------------------------------------------
HERG            GSPPRSAPGQLPSPRAHSLNPDASGSSCSLARTRSRESCASVRRASSADDIEAMRAGVLP 297
mHCN2           ------------------------------------------------------------
MlotiK          ------------------------------------------------------------

                                              <---BD-N--->
mEAG            ----------------------------------KFARLTRALTSSRGVLQQLAPSVQ-- 173
hEAG            ----------------------------------KFARLTRALTSSRGVLQQLAPSVQ-- 173
HERG            PPPRHASTGAMHPLRSGLLNSTSDSDLVRYRTISKIPQITLNFVDLKGDPFLASPTSDRE 357
mHCN2           ----------------------------------EPRGSQASFLQRQFGALLQPGVN-- 149
MlotiK          ------------------------------------------------------------

                                                  |---------------S1---
mEAG            ------KGENVHKHSRLAEVLQLGSDILPQYKQEAPKTPPHIILHYCVFKTTWDWIILIL 227
hEAG            ------KGENVHKHSRLAEVLQLGSDILPQYKQEAPKTPPHIILHYCVFKTTWDWIILIL 227
HERG            IIAPKIKERTHNVTEKVTQVLSLGADVLPEYKLQAPRIHRWTILHYSPFKAVWDWLILLL 417
mHCN2           ---------------KFSLRMFGSQKAVEREQERVKSAGAWIIHPYSDFRFYWDFTMLLF 194
MlotiK          --------------MSVLPFLRIYAPLNAVLAAPGLLAVAALTIPDMSGRSRLALAALLA 46
                              .   :                                :      *:

                 --------|                         |---------S2---------|
mEAG            TFYTAILVPYNVSFKTRQNN------------VAWLVVDSIVDVIFLVDIVLNFHT-TFV 274
hEAG            TFYTAILVPYNVSFKTRQNN------------VAWLVVDSIVDVIFLVDIVLNFHT-TFV 274
HERG            VIYTAVFTPYSAAFLLKETEEGPPATECGYACQPLAVVDLIVDIMFIVDILINFRT-TYV 476
mHCN2           MVGNLIIIPVGITFFKDETT------------APWIVFNVVSDTFFLMDLVLNFRTGIVI 242
MlotiK          VIWGAYLLQLAATLLKRRAG----------------------VVRDRTPKIAIDVLAVL 83
                 .    :     ::   .                              .      : : .   :

                                |-------S3--------|
mEAG            GPAGEVISDPKLIRMNYLKTWFVIDLLSCLPYDVINAFENVDEVSAFMGDPGKIGFADQI 334
hEAG            GPAGEVISDPKLIRMNYLKTWFVIDLLSCLPYDVINAFENVDEG---------------- 318
HERG            NANEEVVSHPGRIAVHYFKGWFLIDMVAAIPFDLLIFGS--------------------- 515
mHCN2           EDNTEIILDPEKIKKKYLRTWFVVDFVSSIPVDYIFLIVEKG----------------- 284
```

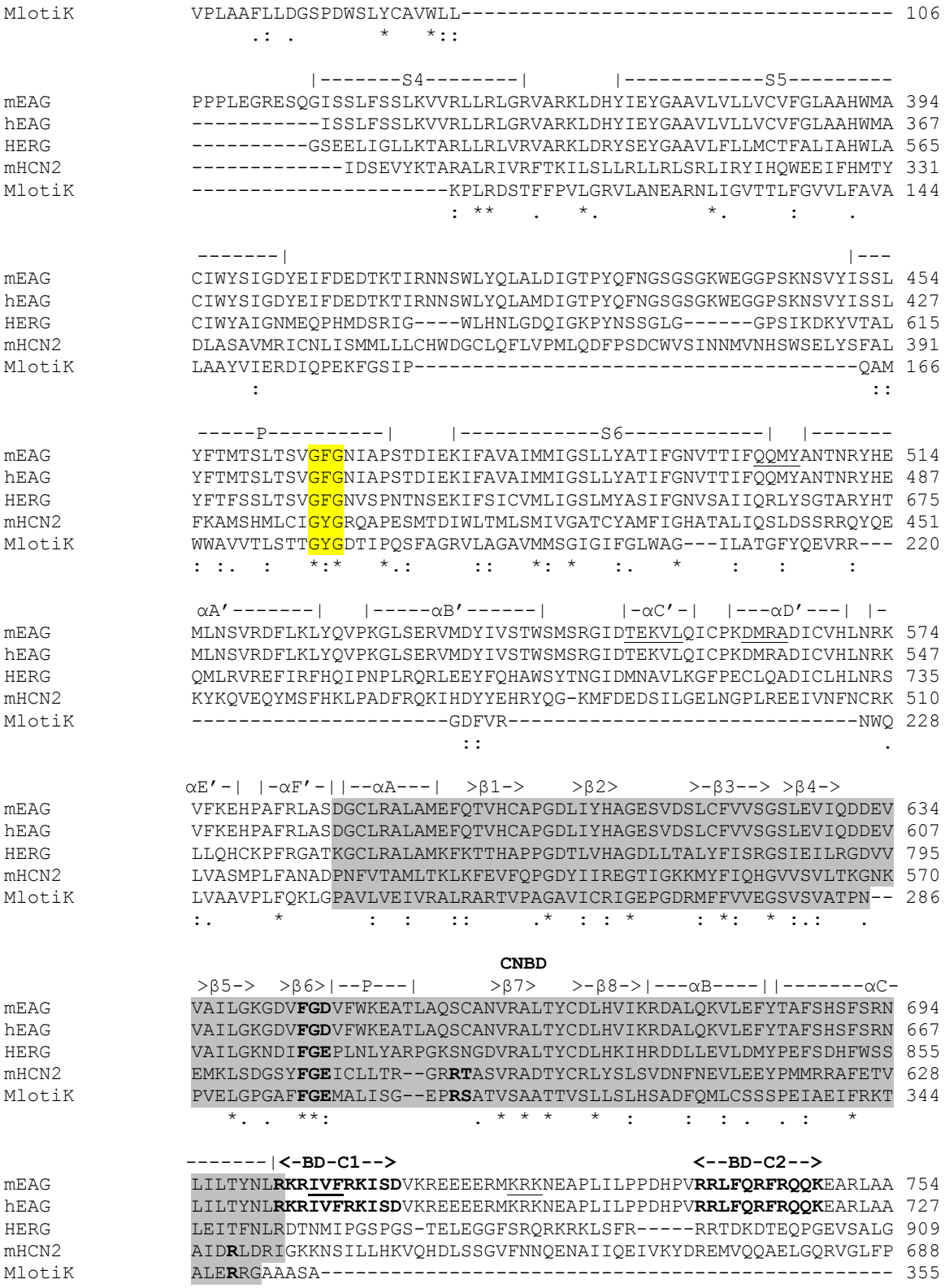
MlotiK VPLAAFLLDGSPDWSLYCAVWLL---------- 106
|-------S4--------| |------------S5---------
mEAG PPPLEGRESQGISSLFSSLKVVRLLRLGRVARKLDHYIEYGAAVLVLLVCVFGLAAHWMA 394
hEAG -----------ISSLFSSLKVVRLLRLGRVARKLDHYIEYGAAVLVLLVCVFGLAAHWMA 367
HERG ----------GSEELIGLLKTARLLRLVRVARKLDRYSEYGAAVLFLLMCTFALIAHWLA 565
mHCN2 -------------IDSEVYKTARALRIVRFTKILSLLRLLRLSRLIRYIHQWEEIFHMTY 331
MlotiK ----------KPLRDSTFFPVLGRVLANEARNLIGVTTLFGVVLFAVA 144
-------| |---
mEAG CIWYSIGDYEIFDEDTKTIRNNSWLYQLALDIGTPYQFNGSGSGKWEGGPSKNSVYISSL 454
hEAG CIWYSIGDYEIFDEDTKTIRNNSWLYQLAMDIGTPYQFNGSGSGKWEGGPSKNSVYISSL 427
HERG CIWYAIGNMEQPHMDSRIG----WLHNLGDQIGKPYNSSGLG------GPSIKDKYVTAL 615
mHCN2 DLASAVMRICNLISMMLLLCHWDGCLQFLVPMLQDFPSDCWVSINNMVNHSWSELYSFAL 391
MlotiK LAAYVIERDIQPEKFGSIP----------QAM 166
-----P----------| |------------S6------------| |-------
mEAG YFTMTSLTSVGFGNIAPSTDIEKIFAVAIMMIGSLLYATIFGNVTTIFQQMYANTNRYHE 514
hEAG YFTMTSLTSVGFGNIAPSTDIEKIFAVAIMMIGSLLYATIFGNVTTIFQQMYANTNRYHE 487
HERG YFTFSSLTSVGFGNVSPNTNSEKIFSICVMLIGSLMYASIFGNVSAIIQRLYSGTARYHT 675
mHCN2 FKAMSHMLCIGYGRQAPESMTDIWLTMLSMIVGATCYAMFIGHATALIQSLDSSRRQYQE 451
MlotiK WWAVVTLSTTGYGDTIPQSFAGRVLAGAVMMSGIGIFGLWAG---ILATGFYQEVRR--- 220
αA'-------| |-----αB'------| |-αC'-| |---αD'---| |-
mEAG MLNSVRDFLKLYQVPKGLSERVMDYIVSTWSMSRGIDTEKVLQICPKDMRADICVHLNRK 574
hEAG MLNSVRDFLKLYQVPKGLSERVMDYIVSTWSMSRGIDTEKVLQICPKDMRADICVHLNRK 547
HERG QMLRVREFIRFHQIPNPLRQRLEEYFQHAWSYTNGIDMNAVLKGFPECLQADICLHLNRS 735
mHCN2 KYKQVEQYMSFHKLPADFRQKIHDYYEHRYQG-KMFDEDSILGELNGPLREEIVNFNCRK 510
MlotiK ----------GDFVR----------NWQ 228
αE'-| |-αF'-||--αA---| >β1-> >β2> >-β3--> >β4->
mEAG VFKEHPAFRLASDGCLRALAMEFQTVHCAPGDLIYHAGESVDSLCFVVSGSLEVIQDDEV 634
hEAG VFKEHPAFRLASDGCLRALAMEFQTVHCAPGDLIYHAGESVDSLCFVVSGSLEVIQDDEV 607
HERG LLQHCKPFRGATKGCLRALAMKFKTTHAPPGDTLVHAGDLLTALYFISRGSIEILRGDVV 795
mHCN2 LVASMPLFANADPNFVTAMLTKLKFEVFQPGDYIIREGTIGKKMYFIQHGVVSVLTKGNK 570
MlotiK LVAAVPLFQKLGPAVLVEIVRALRARTVPAGAVICRIGEPGDRMFFVVEGSVSVATPN-- 286
CNBD
>β5-> >β6>|--P---| >β7> >-β8->|---αB----||-------αC-
mEAG VAILGKGDVFGDVFWKEATLAQSCANVRALTYCDLHVIKRDALQKVLEFYTAFSHSFSRN 694
hEAG VAILGKGDVFGDVFWKEATLAQSCANVRALTYCDLHVIKRDALQKVLEFYTAFSHSFSRN 667
HERG VAILGKNDIFGEPLNLYARPGKSNGDVRALTYCDLHKIHRDDLLEVLDMYPEFSDHFWSS 855
mHCN2 EMKLSDGSYFGEICLLTR--GRRTASVRADTYCRLYSLSVDNFNEVLEEYPMMRRAFETV 628
MlotiK PVELGPGAFFGEMALISG--EPRSATVSAATTVSLLSLHSADFQMLCSSSPEIAEIFRKT 344
-------|<-BD-C1--> <--BD-C2-->
mEAG LILTYNLRKRIVFRKISDVKREEEERMKRKNEAPLILPPDHPVRRLFQRFRQQKEARLAA 754
hEAG LILTYNLRKRIVFRKISDVKREEEERMKRKNEAPLILPPDHPVRRLFQRFRQQKEARLAA 727
HERG LEITFNLRDTNMIPGSPGS-TELEGGFSRQRKRKLSFR-----RRTDKDTEQPGEVSALG 909
mHCN2 AIDRLDRIGKKNSILLHKVQHDLSSGVFNNQENAIIQEIVKYDREMVQQAELGQRVGLFP 688
MlotiK ALERRGAAASA---------- 355
mEAG ERGGRDLDDLDVEKGNALTDHTSANHSLVKASVVTVRESPATPVSFQAATTSTMSDHAKL 814
hEAG ERGGRDLDDLDVEKGNVLTEHASANHSLVKASVVTVRESPATPVSFQAASTSGVPDHAKL 787
HERG PGRAGAGPSSRGRPGGPWGESPSSGPSSPESSEDEGPGRSSSPLRLVPFSSPRPPGEPPG 969
mHCN2 P----------PPPPQVTSAIATLQQAVAMSFCPQVARPLVGPLAL 724
MlotiK ----------

```
mEAG            HAPGSECLGPKAVSCDPAK--RKGWARFKDACGKGEDWNKVSKAESMETLPERTKAPGEA 872
hEAG            QAPGSECLGPKGGGGDCAK--RKSWARFKDACGKSEDWNKVSKAESMETLPERTKASGEA 845
HERG            GEPLMEDCEKSSDTCNPLSGAFSGVSNIFSFWGDSRGRQYQELPRCPAPTPSLLNIPLSS 1029
mHCN2           GSPRLVRRAPPGPLPPAAS--------------------PGPPAASPPAAPSSPRAPRTS 764
MlotiK          ------------------------------------------------------------

mEAG            TLKKTDSCDSGITKSDLRLDNVGETRSPQDRSPILAEVKHSFYPIPEQTLQATVLEVKYE 932
hEAG            TLKKTDSCDSGITKSDLRLDNVGEARSPQDRSPILAEVKHSFYPIPEQTLQATVLEVRHE 905
HERG            PGRRPRGDVESRLDALQRQLNRLETRLSADMATVLQLLQRQMTLVPPAYSAVTTPGPGPT 1089
mHCN2           PYGVPGS----------PATRVGPALPARRLSRASRPLSASQPSLPHGVPAPSPAASARP 814
MlotiK          ------------------------------------------------------------

mEAG            LKEDIKALNAKMTSIEKQLSEILRILMSRGSAQSPQETGEISRPQSPESDRDIFGAS--- 989
hEAG            LKEDIKALNAKMTNIEKQLSEILRILTSRRSSQSPQELFEISRPQSPESERDIFGAS--- 962
HERG            STSPLLPVSPLPTLTLDSLSQVSQFMACEELPPGAPELPQEGPTRRLSLPGQLGALTSQP 1149
mHCN2           ASSSTPRLGPAPTARTAAPSPDRRDSASPGAASGLDPLDSARSRLSSNL---------- 863
MlotiK          ------------------------------------------------------------

mEAG            ----------
hEAG            ----------
HERG            LHRHGSDPGS 1159
mHCN2           ----------
MlotiK          ----------
```

Multiple sequence alignment of C-linker (αA'-αF'), CNBD, BD-C1 and BD-C2 of mEAG

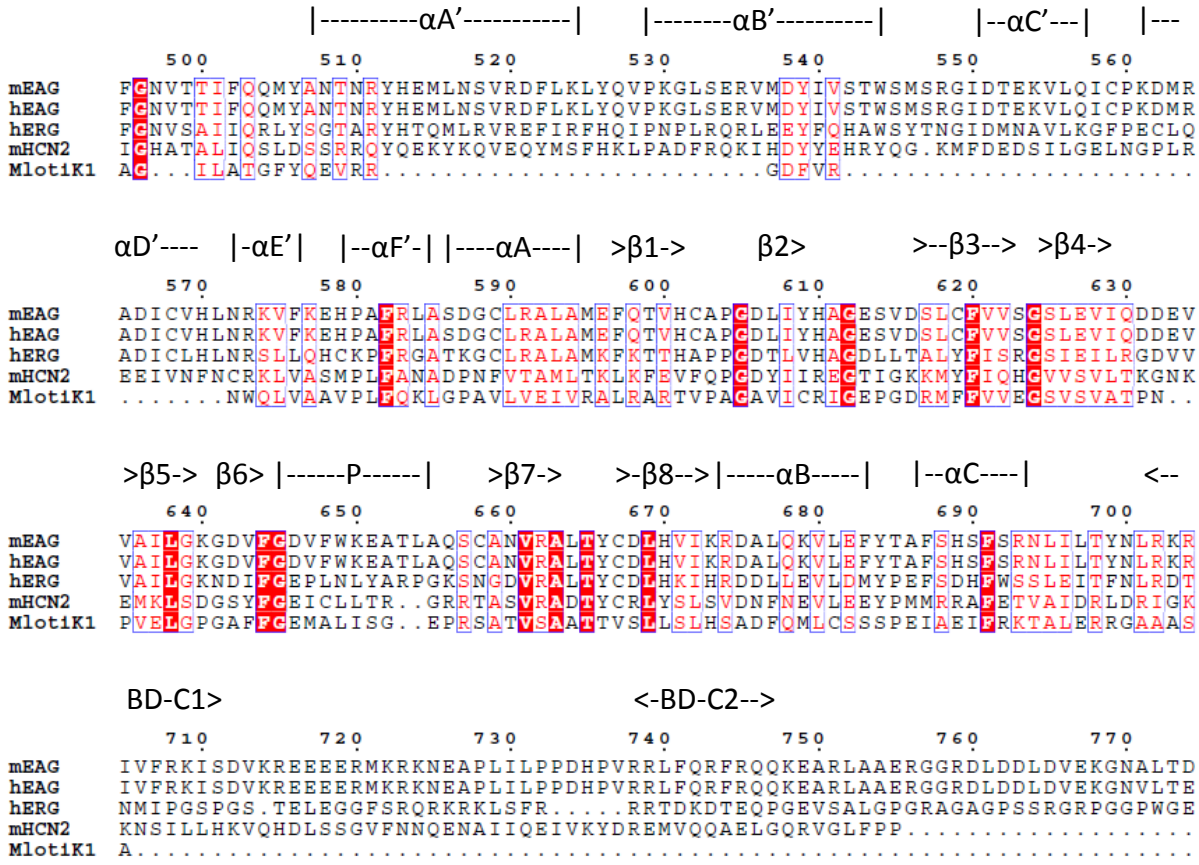

Appendix II - mEAG full sequence

LOCUS NP_034730 989 aa linear ROD 13-MAR-2010
DEFINITION potassium voltage-gated channel subfamily H member 1 isoform 1 [Mus musculus].
ACCESSION NP_034730
VERSION NP_034730.1 GI:6754422

CDS 1..989
/gene="Kcnh1"
/gene_synonym="M-eag; MGC124419; MGC124420"
/coded_by="NM_010600.2:137..3106"
/note="isoform 1 is encoded by transcript variant 1"
/db_xref="CCDS:CCDS15627.1"
/db_xref="GeneID:16510"
/db_xref="MGI:1341721"

1 mtmaggrrgl vapqntflen ivrrsndtnf vlgnaqivdw pivysndgfc klsgyhraev
61 mqkssacsfm ygeltdkdtv ekvrqtfeny emnsfeilmy kknrtpvwff vkiapirneq
121 dkvvlflctf sditafkqpi eddsckgwgk farltralts srgvlqqlap svqkgenvhk
181 hsrlaevlql gsdilpqykq eapktpphii lhycvfkttw dwiililtfy tailvpynvs
241 fktrqnnvaw lvvdsivdvi flvdivlnfh ttfvgpagev isdpklirmn ylktwfvidl
301 lsclpydvin afenvdevsa fmgdpgkigf adqipppleg resqgisslf sslkvvrllr
361 lgrvarkldh yieygaavlv llvcvfglaa hwmaciwysi gdyeifdedt ktirnnswly
421 qlaldigtpy qfngsgsgkw eggpsknsvy isslyftmts ltsvgfgnia pstdiekifa
481 vaimmigsll yatifgnvtt ifqqmyantn ryhemlnsvr dflklyqvpk glservmdyi
541 vstwsmsrgi dtekvlqicp kdmradicvh lnrkvfkehp afrlasdgcl ralamefqtv
601 hcapgdliyh agesvdslcf vvsgsleviq ddevvailgk gdvfgdvfwk eatlaqscan
661 vraltycdlh vikrdalqkv lefytafshs fsrnliltyn lrkrivfrki sdvkreeeer
721 mkrkneapli lppdhpvrrl fqrfrqqkea rlaaerggrd lddldvekgn altdhtsanh
781 slvkasvvtv respatpvsf qaattstmsd haklhapgse clgpkavscd pakrkgwarf
841 kdacgkgedw nkvskaesme tlpertkapg eatlkktdsc dsgitksdlr ldnvgetrsp
901 qdrspilaev khsfypipeq tlqatvlevk yelkedikal nakmtsiekq lseilrilms
961 rgsaqspqet geisrpqspe sdrdifgas
//

Appendix III - hCaM full sequence

LOCUS NP_005175 149 aa linear PRI 05-JUL-2010
DEFINITION calmodulin [Homo sapiens].
ACCESSION NP_005175
VERSION NP_005175.2 GI:58218968

CDS 1..149
/gene="CALM3"
/gene_synonym="CALM1; CALM2; PHKD; PHKD3"
/coded_by="NM_005184.2:181..630"
/db_xref="CCDS:CCDS33061.1"
/db_xref="GeneID:808"
/db_xref="HGNC:1449"
/db_xref="HPRD:00243"
/db_xref="MIM:114183"
ORIGIN
1 madqlteeqi aefkeafslf dkdgdgtitt kelgtvmrsl gqnpteaelq dminevdadg
61 ngtidfpefl tmmarkmkdt dseeeireaf rvfdkdgngy isaaelrhvm tnlgekltde
121 evdemiread idgdgqvnye efvqmmtak

Appendix IV - Mass spectra of mEAG 552-724 proteolysis products

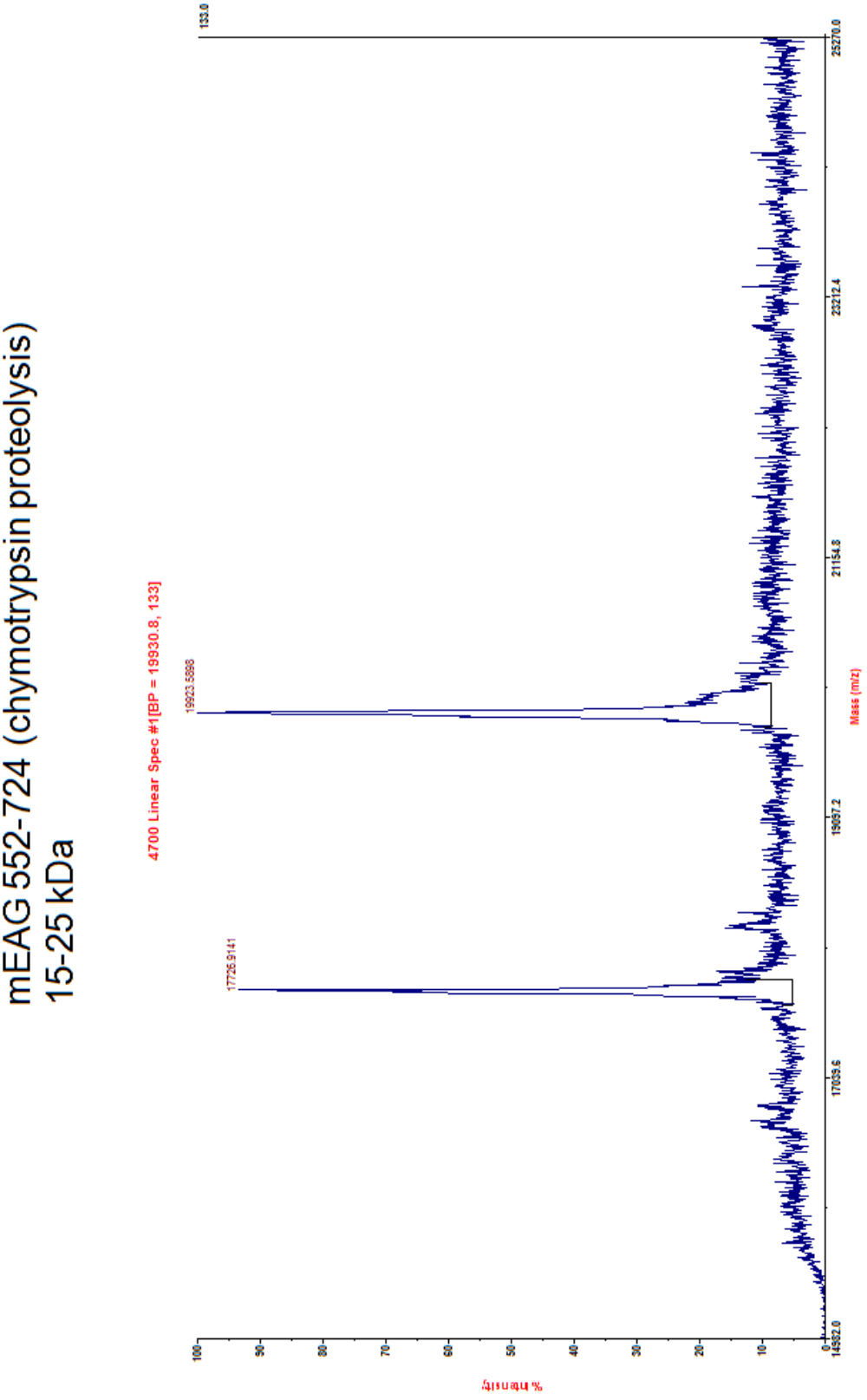

mEAG 552-724 (Lys-C proteolysis)
15-25 kDa

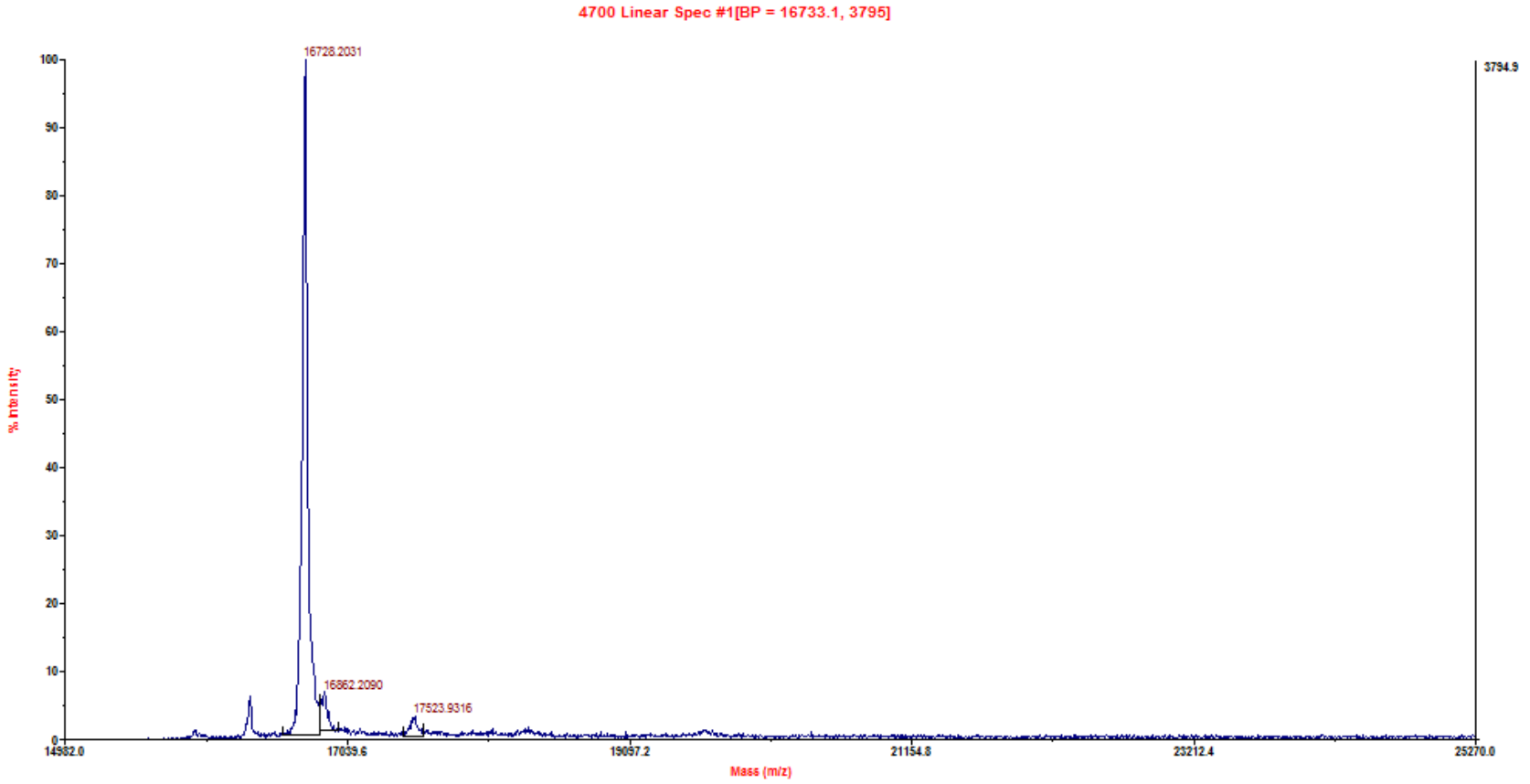

References

1. Lehninger, AL; Nelson, DL; Cox, M. *Lehninger Principles of Biochemistry*. (W.H. Freeman: 2005).

2. Tymoczko, JL; Berg, JM; Stryer, L. *Biochemistry*. (2002).

3. Yellen, G. The voltage-gated potassium channels and their relatives. *Nature* **419**, 35-42(2002).

4. MacKinnon, R. Potassium channels and the atomic basis of selective ion conduction (Nobel Lecture). *Angewandte Chemie (International ed. in English)* **43**, 4265-77(2004).

5. MacKinnon, R. Potassium channels. *FEBS Letters* **555**, 62-65(2003).

6. Doyle, D.A. et al. The structure of the potassium channel: molecular basis of K+ conduction and selectivity. *Science (New York, N.Y.)* **280**, 69-77(1998).

7. Warmke, J., Drysdale, R. & Ganetzky, B. A distinct potassium channel polypeptide encoded by the Drosophila eag locus. *Science (New York, N.Y.)* **252**, 1560-2(1991).

8. Warmke, J.W. & Ganetzky, B. A family of potassium channel genes related to eag in Drosophila and mammals. *Proceedings of the National Academy of Sciences of the United States of America* **91**, 3438-42(1994).

9. Brelidze, T.I., Carlson, A.E. & Zagotta, W.N. Absence of direct cyclic nucleotide modulation of mEAG1 and hERG1 channels revealed with fluorescence and electrophysiological methods. *The Journal of biological chemistry* **284**, 27989-97(2009).

10. Kim, C., Xuong, N.-H. & Taylor, S.S. Crystal structure of a complex between the catalytic and regulatory (RIalpha) subunits of PKA. *Science (New York, N.Y.)* **307**, 690-6(2005).

11. Zagotta, W.N. et al. Structural basis for modulation and agonist specificity of HCN pacemaker channels. *Nature* **425**, 200-5(2003).

12. Clayton, G.M. et al. Structural basis of ligand activation in a cyclic nucleotide regulated potassium channel. *Cell* **119**, 615-27(2004).

13. Clayton, G.M. et al. Structure of the transmembrane regions of a bacterial cyclic nucleotide-regulated channel. *Proceedings of the National Academy of Sciences of the United States of America* **105**, 1511-5(2008).

14. Zhou, L. & Siegelbaum, S.A. Gating of HCN channels by cyclic nucleotides: residue contacts that underlie ligand binding, selectivity, and efficacy. *Structure (London, England : 1993)* **15**, 655-70(2007).

15. Kannan, N. et al. Evolution of allostery in the cyclic nucleotide binding module. *Genome biology* **8**, R264(2007).

16. Altieri, S.L. et al. Structural and energetic analysis of activation by a cyclic nucleotide binding domain. *Journal of molecular biology* **381**, 655-69(2008).

17. Rehmann, H., Wittinghofer, A. & Bos, J.L. Capturing cyclic nucleotides in action: snapshots from crystallographic studies. *Nature reviews. Molecular cell biology* **8**, 63-73(2007).

18. Stansfeld, C.E. et al. Elevation of intracellular calcium by muscarinic receptor activation induces a block of voltage-activated rat ether-à-go-go channels in a stably transfected cell line. *Proceedings of the National Academy of Sciences of the United States of America* **93**, 9910-4(1996).

19. Schönherr, R., Löber, K. & Heinemann, S.H. Inhibition of human ether à go-go potassium channels by Ca(2+)/calmodulin. *The EMBO journal* **19**, 3263-71(2000).

20. Ziechner, U. et al. Inhibition of human ether à go-go potassium channels by Ca2+/calmodulin binding to the cytosolic N- and C-termini. *The FEBS journal* **273**, 1074-86(2006).

21. Gonçalves, J.T. & Stühmer, W. Calmodulin interaction with hEAG1 visualized by FRET microscopy. *PloS one* **5**, e10873(2010).

22. Ausubel, F.M. et al. *Current Protocols in Molecular Biology*. *Molecular Biology* (John Wiley & Sons, Inc: 2003).

23. Strasburg, G.M. et al. Site-specific derivatives of wheat germ calmodulin. Interactions with troponin and sarcoplasmic reticulum. *The Journal of biological chemistry* **263**, 542-8(1988).

24. Sanderson, M; Skelly, J. *Macromolecular crystallography: conventional and high-throughput methods*. *Methods in enzymology* (Oxford University Press: 2007).

25. McPherson, A. Current approaches to macromolecular crystallization. *European journal of biochemistry / FEBS* **189**, 1-23(1990).

26. Coligan, J.E.; Dunn, B.M.; Ploegh, H.L.; Speicher, D.W.; Wingfield, P.T. *Current protocols in protein science*. *Proteins: Structure, Function, and Genetics* **24**, (John Wiley and Sons, Inc.: 2007).

27. Garman, E. “Cool” crystals: macromolecular cryocrystallography and radiation damage. *Current Opinion in Structural Biology* **13**, 545-551(2003).

28. Garman, E.F. & Schneider, T.R. Macromolecular Cryocrystallography. *Journal of Applied Crystallography* **30**, 211-237(1997).

29. Collaborative Computational Project, N.4 The CCP4 suite: programs for protein crystallography. *Acta crystallographica. Section D, Biological crystallography* **50**, 760-3(1994).

30. Adams, P.D. et al. PHENIX: a comprehensive Python-based system for macromolecular structure solution. *Acta crystallographica. Section D, Biological crystallography* **66**, 213-21(2010).

31. Painter, J. & Merritt, E. a Optimal description of a protein structure in terms of multiple groups undergoing TLS motion. *Acta crystallographica. Section D, Biological crystallography* **62**, 439-50(2006).

32. Emsley, P. & Cowtan, K. Coot: model-building tools for molecular graphics. *Acta crystallographica. Section D, Biological crystallography* **60**, 2126-32(2004).

33. Dong, A. et al. In situ proteolysis for protein crystallization and structure determination. *Nature methods* **4**, 1019-21(2007).

34. Wernimont, A. & Edwards, A. In situ proteolysis to generate crystals for structure determination: an update. *PloS one* **4**, e5094(2009).

35. Kincaid, R.L., Billingsley, M.L. & Vaughan, M. Preparation of fluorescent, cross-linking, and biotinylated calmodulin derivatives and their use in studies of calmodulin-activated phosphodiesterase and protein phosphatase. *Methods in enzymology* **159**, 605-26(1988).

36. Kincaid, R.L. et al. Ca2+-dependent interaction of 5-dimethylaminonaphthalene-1-sulfonyl-calmodulin with cyclic nucleotide phosphodiesterase, calcineurin, and troponin I. *The Journal of biological chemistry* **257**, 10638-43(1982).

37. Kelley, L. a & Sternberg, M.J.E. Protein structure prediction on the Web: a case study using the Phyre server. *Nature protocols* **4**, 363-71(2009).

38. Bauer, C.K. & Schwarz, J.R. Physiology of EAG K+ channels. *The Journal of membrane biology* **182**, 1-15(2001).